RASA REPORT 72-04

AN INVESTIGATION OF THE MIXING OF LINEAR AND SWIRLING FLOWS

Final Technical Report for the Period
15 February 1971 - 14 February 1972

by

Richard P. White, Jr.
John C. Balcerak

Prepared Under Contract No. N00014-71-C-0226
Req. No. NR215-170/10-30-70(Code 461)
by

ROCHESTER APPLIED SCIENCE ASSOCIATES, INC.
140 Allens Creek Road, Rochester, New York 14618
716/271-3450

for

OFFICE OF NAVAL RESEARCH
AERONAUTICS, CODE 461
DEPARTMENT OF THE NAVY
Arlington, Virginia 22217

ACKNOWLEDGMENTS

The authors wish to express their appreciation to Dr. Keith W. Shipman for his assistance in the conduct of the experiments, and to Dr. Stephen A. Rinehart and Mr. Lawrence R. Sutton for their help in conducting the experiments and in developing an extended theory and correlating the theoretical results with those obtained during the experimental phase of the investigation.

UNCLASSIFIED
Security Classification

DOCUMENT CONTROL DATA - R & D

(Security classification of title, body of abstract and indexing annotation must be entered when the overall report is classified)

1. ORIGINATING ACTIVITY (Corporate author)	2a. REPORT SECURITY CLASSIFICATION
ROCHESTER APPLIED SCIENCE ASSOCIATES, INC. 140 Allens Creek Road Rochester, New York 14618	UNCLASSIFIED 2b. GROUP N/A

3. REPORT TITLE

AN INVESTIGATION OF THE MIXING OF LINEAR AND SWIRLING FLOWS

4. DESCRIPTIVE NOTES (Type of report and inclusive dates)

Final Technical Report - 15 February 1971 - 14 February 1972

5. AUTHOR(S) (First name, middle initial, last name)

Richard P. White, Jr.; John C. Balcerak

6. REPORT DATE	7a. TOTAL NO. OF PAGES	7b. NO. OF REFS
February 1972	77	14

8a. CONTRACT OR GRANT NO.	9a. ORIGINATOR'S REPORT NUMBER(S)
N00014-71-C-0226 b. PROJECT NO. c. d.	72-04 9b. OTHER REPORT NO(S) (Any other numbers that may be assigned this report)

10. DISTRIBUTION STATEMENT

Approved for public release; distribution unlimited

11. SUPPLEMENTARY NOTES	12. SPONSORING MILITARY ACTIVITY
	Office of Naval Research Aeronautics, Code 461 Arlington, Virginia 22217

13. ABSTRACT

A research program was conducted to study in detail the importance of various aerodynamic and geometric parameters on the dissipation of a concentrated trailed vortex in which the dissipation is greatly enhanced by the continuous injection of a mass of air into its core.

The basic results of the research program demonstrated that the efficiency of vortex dissipation would be maximized by designing the injection system so that the vortex was injected at its center and parallel to the axis of the trailed vortex core with a linearly-directed mass of air at sonic speeds. The efficiency of the optimum system was shown to be almost an order of magnitude better than had been demonstrated previously. The theoretical analysis that was developed closely correlated the experimental results and can be used to predict the effect of the controlling parameters of the injection nozzle on the dissipation of the vortex as a function of the distance from the trailing edge of the airfoil. (U)

DD FORM 1 NOV 68 1473 REPLACES DD FORM 1473, 1 JAN 64, WHICH IS OBSOLETE FOR ARMY USE.

UNCLASSIFIED
Security Classification

14. KEY WORDS	LINK A		LINK B		LINK C	
	ROLE	WT	ROLE	WT	ROLE	WT
Aerodynamics						
Rotor Blades						
Tip Vortex						
Viscous Mixing						
Swirling Flow						
Mass Flow Injection						

ABSTRACT

A research program was conducted to study in detail the importance of various aerodynamic and geometric parameters on the dissipation of a concentrated trailed vortex in which the dissipation is greatly enhanced by the continuous injection of a mass of air into its core.

The basic results of the research program demonstrated that the efficiency of vortex dissipation would be maximized by designing the injection system so that the vortex was injected at its center and parallel to the axis of the trailed vortex core with a linearly-directed mass of air at sonic speeds. The efficiency of the optimum system was shown to be almost an order of magnitude better than had been demonstrated previously. The theoretical analysis that was developed closely correlated the experimental results and can be used to predict the effect of the controlling parameters of the injection nozzle on the dissipation of the vortex as a function of the distance from the trailing edge of the airfoil.

TABLE OF CONTENTS

LIST OF SYMBOLS

a_j	initial radius of injection jet (ft)
a_∞	speed of sound (ft/sec)
c	chord of lifting surface (ft)
C_L	coefficient of lift (nondimensional)
C_ℓ	section lift coefficient
C_p	coefficient of pressure (nondimensional)
C_μ	jet momentum coefficient
h	slot height (ft)
M	Mach number
M_∞	freestream Mach number
m	mass efflux per unit length (slugs/sec-ft)
m_i	weight of injected air per second (lb/sec)
q_∞	freestream dynamic pressure (lb/ft^2)
r_c	initial radius of vortex core (ft)
V_j	injection velocity (ft/sec)
V_∞	freestream velocity (ft/sec)
x	downstream distance from trailing edge of lifting surface (ft)
ε_0	coefficient of kinematic eddy viscosity
ρ	density of air ($slug^2/ft^3$)
Γ	vortex circulation strength (ft^2/sec)
Γ_0	initial vortex circulation strength (ft^2/sec)

LIST OF FIGURES

LIST OF FIGURES

LIST OF FIGURES

I. INTRODUCTION

When an airfoil surface develops lift, a considerable amount of energy is deposited in the fluid in which the lifting surface is operating. Generally this energy is concentrated in a relatively small volume commonly referred to as the tip vortex which streams away from the tip of the airfoil. The nonuniform induced flow field developed by the tip vortex of a helicopter blade has been of considerable concern to the rotary-wing aerodynamicist, dynamicist, and acoustician because of the turbulent flow field that is created which causes high dynamic blade loads and acoustic problems. Helicopter blade-vortex interaction has been of considerable concern as regards blade loading and dynamic response as well as regards noise associated with impulsive loading such as "blade slap". These characteristic noise signatures are of particular importance in detection problems associated with military operations and in annoyance problems associated with civil operations.

While the nonuniform induced flow field created by the tip vortex emanating from the helicopter rotor blades in forward flight has been of considerable concern to the developers and users of helicopters and V/STOL aircraft for many years, it has not, in the past, been of primary concern to the manufacturers and users of fixed-wing aircraft. This previous lack of serious concern was probably fostered by the fact that the vortex flow field created by a fixed lifting surface in forward flight generally did not create any significant problems to the airfoil that created it. A primary exception to this, of course, was the vortex interaction problems associated with highly pointed delta wings at angle of attack. During the past few years, however, because of the higher frequency of departures and landings at airports involving both large and small aircraft, the important and deleterious effects of the tip vortex generated by the larger aircraft on smaller aircraft flying through or in the proximity of the trailed vortex, has become a problem

of great concern. During recent conferences on the effects of aircraft-generated wake turbulences (Refs. 1 and 2), the serious effects of the tip vortex created by the 747 and C-5A in a landing or approach configuration on the control and stability characteristics of following aircraft as large as the 737 were illustrated and discussed in great depth. It can be concluded, therefore, that the extreme deleterious effects of the tip vortex generated by a lifting surface, either rotating or non-rotating, are present for all forms of aircraft and thus investigations to alleviate these effects are no' only timely but important and universal.

Numerous research efforts have been conducted in the past by various investigators to alter the characteristics of the tip vortex and thus alleviate the blade response and noise problem associated with helicopters. Several approaches have been employed, including modification of the loading distribution by taper and twist and altering the tip geometry by using porous sections. All of these approaches, while sometimes achieving a moderate degree of success at a given flight condition, have not been successful for all flight conditions. On the other hand, very little has been done to determine what can be accomplished to alter the trailing vortex from fixed-wing aircraft.

RASA believed, based on previous research in which it was engaged, that injecting a linearly-directed aerodynamic mass flow into the core of a swirling tip vortex would significantly increase the viscous dissipation of that vortex. This vortex modification technique has the sole objective of rapidly dissipating the strength of the concentrated vorticity, by the action of eddy viscosity at the lower mass flows or by the generation of a jet flow instability at the higher mass flows.

Under ONR sponsorship, RASA conducted a theoretical analysis (Ref. 3) of the mixing of such an injected air flow in the core of the vortex. The results of this theoretical work were extremely encouraging in that they indicated that the concentrated

vorticity of the trailed tip vortex could be significantly reduced by the input of a relatively small amount of mass flow into the core of the vortex. The analysis also indicated that the performance parameters, such as lift and drag, would not be affected to any degree and that, furthermore, the required mass flow was low enough that in helicopter rotor systems, it could probably be obtained through centrifugal pumping in the rotor system. This theoretical research program also investigated the effects of suction and reverse swirl on the modification of the tip vortex, but found that neither of these approaches were practical or beneficial.

In view of the encouraging results of this theoretical research, ONR sponsored an experimental program with RASA to determine if the predicted beneficial results of vortex injection were in fact realizable. The results of this experimental program (Ref. 4) generally confirmed the theoretical predictions up to specific values of injected flow. Beyond that, where the theory could not account for large-scale flow turbulence, the experimental results were even more encouraging than that of the theory. Thus, it appeared that modification of the vortex problem at its source could be realized, not only in the helicopter industry but also in the fixed-wing industry.

In order to place the results of the previous ONR-RASA research programs in the proper context in regard to the research program that is reported on herein, a few of the more pertinent experimental results obtained by RASA in the previous experimental program (Ref. 4) are presented and discussed. In Reference 4, the vorticity contours that were measured at 6-1/2 chordlengths behind the model showed that the magnitude of the vorticity was reduced by a factor of approximately 10 at the highest mass flow tested. At 1-1/2 chordlengths behind the model, the magnitude of the vorticity at this mass flow rate was also reduced, but to a much smaller degree. The changes in the circulation strengths of the vortices with injected mass flow based on integrations of the vorticity distributions were

compared with the changes in the circulation strengths predicted by the theory of Reference 3. The agreement between theory and experiment up to given mass flows was extremely good, but above this mass flow the experimental results indicated a much larger dissipation than had been predicted by theory. The point at which the theory started to deviate from the experimental results was correlated with a vortex-breakdown parameter developed during basic investigations of vortex breakdown on delta wings. While this correlation did not prove that vortex breakdown was initiated by mass injection, the correlation strongly suggested that an instability was at the heart of the difference between theory and experiment with higher mass flows. The existence of an instability provided a possible explanation as to why the predicted results indicated a less favorable dissipation than was measured. The theory, which was based on the dissipative action of eddy viscosity and not vortex stability, used as input an averaged eddy viscosity constant as determined by Schlicting. If, however, three-dimensional, jet-vortex instability occurred, the turbulence wavelength would be radically altered and the effective eddy viscosity constant would be much larger than that before vortex breakdown occurred. If an instability did occur, and the eddy viscosity coefficient could be determined and used in the theory, correlation at the higher mass might be realized.

Unfortunately, the initial test program could not conduct the detailed investigation of the mixing of linear and swirling flows that was required to determine if viscous dissipation or vortex instability was the mechanism by which the vortex flow was more effectively eliminated downstream of the airfoil. Since it was either more effective turbulent mixing or a vortex instability that seemed to yield a more beneficial effect than that predicted, it was believed important to conduct a more detailed investigation of the mixing phenomenon to either improve the assumption of the present turbulent viscous-mixing theory or to uncover the different mechanism by which the more

beneficial effects were obtained. In addition, since circulation-controlled rotors could also be of benefit in this regard if they are properly designed in the tip region, it was believed important that the results that were obtained be evaluated in light of the characteristics of circulation-controlled rotors to determine if, by proper design, these type of rotor systems could also beneficially modify the tip vortex which they generate. These above-mentioned objectives were the subject of the research program that is reported on in this report.

II. DEVELOPMENT OF THEORETICAL ANALYSIS

During a previous investigation conducted by Rochester Applied Science Associates, Inc. for the Office of Naval Research (Ref. 4), it was determined experimentally that axial-flow injection could markedly alter the vortex core structure and velocity distributions by rapidly spreading and dissipating the concentrated vorticity. It was believed that the rapid dissipation of vorticity of the vortex core could have resulted from a "kink" instability created in the tip vortex core by the turbulent jet. Therefore, on the basis of the results obtained in the test program, an effort was initiated to study the mixing of a linear and a swirling flow in an aerodynamic medium to obtain a better understanding of the flow parameters involved.

Mixing of linear and swirling flows generally result in a turbulent flow field. The study that is reported on herein was concerned with the fluctuations which are superimposed by a jet of fluid on the primary swirling motion. The fluctuations are extremely complex in their details but the resulting mixing motions are very important for the equilibrium of forces.

The turbulent mixing process between the linear and swirling flows is responsible for the continuous transport of energy from the main swirling flow into large eddies. The presence of viscosity results in the dissipation of energy which is finally transformed into heat. As a consequence of the random turbulent mixing processes created by a jet of fluid injected into a swirling flow field, experimental results (Ref. 4) suggest that there is an increased eddy viscosity which greatly enhances the dissipation of the swirling flow field. The results caused by injecting a jet of fluid are as if the ordinary laminar viscosity was increased by a factor of one thousand or more.

Originally, Rinehart (Ref. 3) proposed an eddy viscosity model to study the effects of injecting a vortex core with a

linearly-directed mass of air. Preliminary correlations with experimental data suggested that the approach had merit and that such a theoretical model could be used to predict gross changes occurring in the circulation strength associated with a fully developed free-turbulent flow field. Initial computations with the theoretical model were based on Schlicting's expression for the eddy viscosity (assumed constant) of a quiescent jet (Ref. 5).

It had been noted upon examination of the experimental data on injected turbulent flows, that the circulation profiles under consideration could be approximated very successfully by Gauss' function. Starting from this premise, an effort was made to cover all cases of turbulent injected vortices by proceeding in a reverse direction and formulating an inductive theory with the aid of a simple set of equations instead of endeavoring to solve the complete set of differential equations of fluid dynamics.

The Navier-Stokes equations for a steady-state, turbulent, incompressible flow field are given as follows:

$$(\bar{v} \cdot \text{grad})\bar{v} = -\frac{\text{grad}\, p}{\rho} + \varepsilon_0 \nabla^2 \bar{v}, \quad \text{div}\ \bar{v} = 0 \qquad (1)$$

in which ε_0 is the turbulent eddy coefficient of viscosity. By assuming that the dependent variables change much more rapidly in the radial direction than in a downstream or axial direction, and assuming that the radial flow component is small as compared with the axial component (i.e., boundary-layer approximations), that is,

$$\frac{\partial}{\partial x} \ll \frac{\partial}{\partial r}\ ,\ \bar{v}_r \ll \bar{v}_x \text{ (cylindrical coordinates)}$$

the axisymmetric equation of motion for the circulation for an injected vortex can be written as follows:

$$V_\infty \frac{\partial I}{\partial x} = \varepsilon_0(x) r \frac{\partial}{\partial r}\left(\frac{1}{r}\frac{\partial I}{\partial r}\right) \qquad (2)$$

where $\varepsilon_0(x)$ denotes the eddy viscosity, V_∞ the freestream velocity, and Γ the circulation strength associated with the swirling flow. Thus, the distribution of vorticity in the free turbulent flow field resulting from mixing of linear and swirling unbounded flow fields is governed by a generalized heat conduction equation in which the conductivity (i.e., viscosity) is a function of the axial (streamwise) coordinate. As is well-known from the theory of heat conduction, the solutions of Equation (2) involve the Gauss function. Thus, Equation (2) constitutes a simplified mathematical formula for the circulation profiles in a free turbulent flow provided that $\varepsilon_0(x)$ can be inferred from experimental data. The theory is truly "inductive" in that the development depends upon experimental results to suggest the proper formulation. The asymptotic solution of Equation (2) (Ref. 6) has the form

$$\Gamma = \Gamma_0(1-e^{-\eta}) \tag{3}$$

where

$$\eta = \frac{V_\infty r_c^2}{\varepsilon_0\left(\frac{x}{c}\right)c} \tag{4}$$

and Γ_0 is the initial circulation and r_c is an experimentally determined constant related to vortex core size.

Based upon experimental results, the eddy viscosity ε_0 was assumed to be composed of two terms. One term accounts for the upstream flow field development at the point at which mixing was initiated and included nozzle parameters. The second term incorporated the axial coordinate and was used to account for downstream flow field development (i.e., accounting for such effects as spreading of the jet and entrainment of the surrounding fluid). The expression that accounts for both of these flow effects is given in the following expression:

$$\varepsilon_0 = 0.0155\sqrt{\pi}a_j|V_j-V_\infty|+\alpha_1\left(\frac{r_c}{c}\,x\right)|V_j-V_\infty| \qquad (5)$$

where

ε_0 = kinematic eddy viscosity

a_j = initial jet radius

c = airfoil chord

V_∞ = freestream velocity

V_j = jet velocity at nozzle exit

x = downstream distance from nozzle exit

and r_c and α_1 are determined from experimental data. Using the data presented in Reference (4) the constants r_c/c and α_1 were found to be

$$r_c = 0.085C$$

$$\alpha = 8.0\text{x}10^{-4}$$

Using the measured values of r_c and keeping α_1 a constant, the relations presented in Equation (3), (4), and (5) were used to predict the effect of mass injection on vortex dissipation for all the data obtained in this program. Comparison of the predicted and experimental results are presented in Section V of this report.

III. DESCRIPTION OF MODELS, WIND TUNNEL, INSTRUMENTATION AND WIND TUNNEL TESTS

A. Design of Vortex Generators

The basic phase of the research program was to create a swirling flow field which would closely simulate that which actually occurs in a tip vortex created by a three-dimensional flow field. Initially, it was believed that this flow could be obtained by the use of a one-stage, shrouded-axial vane set in which the angles of attack of the vanes could be varied to control the component of rotational velocity. The implementation of this system within the constraints of the wind tunnel at the University of Rochester proved to be unwieldy, and other methods of generating the swirling flow field were investigated. One of the other possibilities of generating a swirling flow field was the use of a cylindrical vortex chanber or vortex-tube generator. A typical confined vortex configuration of this system consists of a cylindrical chamber with air injected both radially and tangentially at the chamber periphery and withdrawn at the central axis as shown schematically in Figure 1. Various devices that utilize such a vortex configuration include the Ranque-Hilsch tube for heat dissipation, the magnetohydrodynamic vortex generator and the vortex amplifier for fluidics applications. Unfortunately, swirling fluid is removed in the chamber of these devices by central exit tubes of relatively small diameter at the top and bottom of the chambers and thus vortex strength is not preserved. Furthermore, the vortex-tube generators are often operated at very high swirl velocities to increase their efficiency so that radial inflow velocity is negligible compared with tangential (swirl) velocity. In this configuration the axial velocity in the core of the vortex at the vortex chamber outlet would be negligible. In fact, a boundary condition employed by Hornbeck (7) in the analysis of short vortex chambers assumes that the axial velocity in the confined vortex

core at the chamber outlet is zero. Actually, while reliable experimental work has been presented by Savino and Keshock (8) on the radial and tangential velocity distributions in a confined vortex, little information is available on the axial velocity distributions.

On the basis of the study that was conducted, it was believed that the majority of vortex-tube generators did not simulate the ratio of swirl-to-axial velocity which occurs in a tip vortex created by a three-dimensional flow field. This ratio is significant since the axial velocity influences the formation and decay of a vortex strongly, and it could be possible to obtain various decay rates depending on the manner in which the vortex is generated.

Recent detailed experimental results by Chigier (9) showing velocity distributions in the vortex formed by a squared-off wing tip of 18-inch chord at an angle of attack of 12° indicated an excess (greater than freestream) axial velocity in the initial region of the vortex. The maximum axial velocity measured was approximately 1.4 times as great as the freestream velocity. The existence of an excess axial velocity in the vortex core was also predicted theoretically by Rinehart (3) approximately one year before the experimental results of Chigier were obtained. In view of these observations, it was decided to generate vortices in this research program by split-flap type of airfoil configurations which could be mounted in the wind tunnel. Circulation associated with the vortex core could then be varied by varying the included angle of attack of the airfoils and the freestream velocity. For this type of configuration, the proper ratio between swirl and axial velocity could be maintained which would simulate that actually generated by vortices forming over wing tips.

B. Models

The models used in the program were of a NACA 0015 airfoil section with a four-inch chord. The model was machined ir one

piece from a block of solid aluminum, and cut into two 8.24-inch sections so that each section spanned one-half of the test section in the wind tunnel. A schematic sketch of this model is shown in Figure 2. A 3/8-inch diameter hole, centered at the quarter chord, was drilled through the model to provide for the passage of the injected air to the tip of each section.

Each section of the model could be mounted to the floor or ceiling of the test section by bolting through the tunnel plates at the 12.5 percent and 75 percent chord positions. In order to facilitate the installation and alignment of the models for the split-flap tests, dowel pins were inserted at the tip of one section at the 12.5 percent and 75 percent chord positions and matching holes were bored into the other section.

Wind tunnel tests were conducted with the split-flap configurations in which tubes of various dimensions were placed external to the model to provide mass injection. A listing of the tube dimensions and their position in the flow field is shown in Figure 3. Upon completion of the split-flap configuration tests, the end of one of the model sections was modified to accommodate a developed half-round tip and various nozzle configurations. A schematic diagram of a typical nozzle configuration for the single-airfoil tests is shown in Figure 4 and an exploded view of this model and the various nozzles which were used in the single-airfoil tests is shown in Figure 5. A listing of pertinent nozzle data for these tests is given in Figure 6. The nozzle configurations at the leading edge of the model in Figure 5 consist of a series of slots whose outboard edges coincide with the inboard edge of the developed half-round tip cap. The centerlines of the slots at their exits on the contour were located at the 25, 50 and 75 percent chord positions of the model, and the nozzles were machined to direct the injected air at 10 and 15 degrees with respect to the chordline. The exit areas of the slots were 0.1 in.^{2}. Because of physical limitations, however, a nozzle having an exit angle of 10 degrees whose forward edge would be at the 25 percent chord could not be

fabricated. One nozzle was also fabricated with an exit area of 0.1 $in.^2$, an exit angle of 15°, but its spanwise dimension was narrowed to concentrate the injected air nearer the tip. This nozzle is shown at the extreme lower left in Figure 5. A plug was also machined to replace the nozzles and provide an unmodified airfoil section.

The components at the trailing edge of the model in Figure 5 comprise various nozzle configurations whose exit was at the 75 percent chord position and whose exit angle was 15 degrees. The basic interchangeable section shown in the upper right of the photograph comprises a circular nozzle whose diameter was 0.25 in. Tubes of various lengths, which are shown below the nozzle section, could be inserted into the 0.25-inch diameter hole to inject air into the vortex at positions off the airfoil contour. In this program, 1/8- and 3/16-inch I.D. tubes of 1- and 1-1/2-inch lengths were used in various tests.

C. Wind Tunnel

The test phase of the program was conducted in the University of Rochester 16.5" x 24" wind tunnel. The wind tunnel is a closed-return type and operates at four fixed speeds of 75, 115, 150 and 200 fps. The length of the test section is approximately 24 inches and access to the test section is provided by a removable floor section. The other walls of the test section are fixed. Installation of a balance system had not been completed during the course of the test phase of this research program, thus balance data were not obtained during the tests. A photograph of the wind tunnel which also shows the installation of the instrumentation used during the tests is shown in Figure 7, and a schematic diagram of the installation is shown in Figure 8. In the photograph, the model in the test section is obscured by light reflection off the plexiglass walls. A photograph showing the installation of a single-airfoil model and the vortex meter is shown as Figure 9. The console on the right of the photograph (Figure 7) houses the tunnel speed-control switches for the four fixed tunnel speeds.

The vortex meter and the hot wire were mounted onto a traverse mechanism which, in turn, was mounted beneath the floor of the test section. The Xenon lamp for illuminating the helium bubbles was mounted externally at the diffuser section, and the light emanating from the lamp was reflected off a mirror in the diffuser onto the model. The console for controlling the helium-bubble flow can be seen on the table at the left (Figure 7), and readout equipment for the hot wire and vortex meter can be seen on the left of the platform.

D. Instrumentation

The split-flap or single-airfoil models were mounted on the tunnel centerline, and the angle of attack of the model was set and adjusted manually by measuring the offset distance from the tunnel centerline to the trailing edge of the model. Because of the relatively low mass flow injection rates used in the program, the flow rate was determined from calculations based on velocity distributions taken across the jets emanating from the nozzles in terms of various inlet pressure ratios. This method was used as measurement taken with an available flow meter proved to be inaccurate because of the relatively low mass flow rates. Air densities and temperatures at the positions at which the velocities were measured were virtually those of the ambient atmosphere.

The swirl velocities in the trailed tip vortex were monitored by an AEA[1] vortex meter, and the rotational speed of the meter was read out on an electronic counter. The vortex meter was mounted on a two-dimensional, manually-driven traverse mechanism which was suspended beneath the tunnel floor. The traverse mechanism was assembled by mating two UniSlide[2] components. A vernier scale on the components allowed reading positions within 0.001 in., but the resolution on the initial position of the meter was approximately ±0.01 in. The reference positions

[1]Aero Engineering Associates, State College, Pa.
[2]Velmex, Inc., Holcomb, N. Y.

of the vortex meter for the split-flap configuration and the single-airfoil tests were the respective tunnel centerlines.

E. Wind Tunnel Tests

In the first phases of the wind tunnel tests, flow visualization studies were conducted at 75 fps for the split-flap configurations to determine the respective merits of pitching the airfoils at the 12.5 or 75 percent chord positions. On the basis of visual observations and photographs of the flow patterns, it was decided to restrict the quantitative measurements to those split-flap configurations in which the airfoils were pitched about the 12.5 percent chord, for the reasons which will be discussed in Section IV. Wind tunnel tests were then conducted to obtain equal circulation strengths in the vortex at two different wind tunnel speeds by varying the included angle of the split-flap configuration. Various amounts of mass flow were then injected with various external nozzle configurations into the vortices of equal strength which were generated at the two wind tunnel speeds at various chordwise positions to determine the independent effects of the mass rate of injection, the velocity of injection, and the position of the nozzle. Photographs of the flow field were taken in addition to the quantitative measurements.

Upon completion of the split-flap airfoil tests, one of the airfoils was reworked to accommodate a developed half-round tip and various internal nozzles. A developed half-round tip was used in preference to a squared-off or other tip configuration since data on the developed half-round tip were available from other programs under sponsorship of ONR (Ref. 4) and AAMRDL (Ref.10). Wind tunnel tests were then conducted at two speeds to determine the independent effects of the mass rate of injection, the velocity of injection, nozzle position, the angle of injection and the effect of placing the nozzle exit off the contour of the airfoil. Again, photographs of the flow patterns were taken in addition to the quantitative measurements. Spacial limitations precluded the placement of the traverse

mechanism in the diffuser section of the wind tunnel, thus the traverse mechanism was placed as far downstream as possible in the test section. This position was such that the vanes of the vortex meter were approximately 3-1/2 chord-lengths downstream of the trailing edge of the model.

Hot-wire surveys of the wake velocities were made for several configurations using a Thermo-systems, Inc. single wire probe. The signals from the probe were read out on a digital voltmeter. Hot-wire surveys in the wake were limited, however, since the results generally indicated that more sophisticated systems such as three-dimensional probes, would be required to provide adequate quantitative data for the wake surveys.

The hot-wire probe was mounted to the same traverse mechanism as the vortex meter, and its sensor was 4-1/4 chordlengths downstream from the trailing edge of the model since the sensor was at the position of the vertical support rod of the vortex meter (see Figure 9).

Flow visualization studies of the split-flap and single-airfoil tests were provided by neutrally-buoyant helium bubbles[3] which were released upstream of the models. The bubbles were illuminated by a collinated beam of light, observed visually and photographed. The light source for illuminating the bubbles was placed external to the wind tunnel because of its size with respect to that of the wind tunnel, and the light was reflected onto the model off a mirror in the diffuser. Photographs of the bubble streaks were generally taken in the planform view as spacial limitations constrained the camera positions to a narrow spanwise field of view.

---

[3] Hale, R.W., Tan, P., Stowell, R.C., and Ordway, D.E. Development of an Integrated System for Flow Visualization in Air Using Neutrally Buoyant Bubbles, Sage Action Report SAI-RR-7107, December 1971.

IV. DISCUSSION OF RESULTS

A. Split-Flap Vortex Generator Tests

In order to determine the most desirable configuration of the split-flap vortex generator for the purposes of the subject program, the generator was placed in the wind tunnel and flow visualization was used to study the vortex formation as a function of the chordwise location of the pivot point, the included angle of attack, and the freestream velocity. It was determined from these series of tests that the freestream velocity and the included angle of attack were not important parameters in regard to the formation of the vortex field that was generated. It was found, however, that the chordwise location of the pivot point was a very important parameter in regards to the formation of the trailed vortex field. The results of previous research programs showed that the vortex which was formed at the tip of a three-dimensional lifting surface separated from the airfoil surface at the 3/4 chord position and, thus, it was believed that if the two lifting surfaces of the split-flap vortex generator were pivoted relative to each other at that chordwise position, the two independent vortices that were generated would not be affected by the presence of the airfoils. Figure 10 shows the formation of the individual and combined vortices of this configuration at a wind tunnel velocity of 75 ft/sec. The vortex flow field was visualized by concentrating the helium-filled bubbles in the center of the vortex cores with the lifting surfaces at an angle of attack of +15 degrees. It can be seen from the visualized flow that the individual vortices do not start to interact with one another until they have left their respective lifting surfaces. Once the vortices become free vortices, they interact, and because they have the same direction of rotation, they rotate about each other and combine into a single vortex. The single vortex is formed about one and one-half chordlengths downstream of the trailing edge

of the vortex generator. The visualized vortex flow field of the vortex generator at the same freestream velocity and included angle of attack, but with the airfoils pivoted about the 12.5 percent chord is presented in Figure 11. For this configuration it can be seen that the induced vortices begin to interact with each other prior to becoming free vortices and, thus, a single vortex of combined strength begins to form nearer the trailing edge of the airfoil sections, and appears to be completely formed at a location less than one chordlength downstream of the trailing edge. Since physical constraints precluded the mounting of the vortex meter farther downstream than at the end of the test section in the wind tunnel, it was decided to conduct the remainder of the wind-tunnel tests of the split-flap vortex generator with the models pitched about the 12.5 percent chord in order to provide as large a separation as possible between the vortex meter and the point at which a single solid core of rotation was formed in the flow. This separation was 3-1/2 airfoil chordlengths. The largest possible separation was desirable since the effects of mass injection progress with age in the wake, and measurements taken too near the airfoil may not have properly indicated the effects of mass injection on the dissipation of the vortex strength.

During the tests conducted with the split-flap vortex generator, it was noted that the injection tubes which were placed at the center of the lifting surfaces created a certain amount of turbulence which effected some vortex dissipation. Since the diameter and length of the injection tubes effected various amounts of vortex dissipation, measurements of the change in the vortex strength were made with the various injection tubes in place, but with no injected airflow. The results of these measurements are presented in Figure 12. In this figure results are presented for the two freestream velocities used during the test program, and the circulation strength of the vortex as modified by the turbulence generated by each of the injection tubes has been normalized by the strength of the

unmodified vortex. The results show that the increase in the diameter or the length of the injection tube increased the dissipative effect of the nozzle by the turbulence that the nozzle generated. Except for the extended injection tube, the effect of increasing freestream velocity was to cause a greater dissipation of the vortex strength. It is believed that the reason the extended injection tube caused a greater reduction of the vortex strength at 75 ft/sec than at 115 ft/sec is that at the lower freestream velocity, the individual vortices combined more rapidly, that is, at downstream distances closer to the airfoil, and thus the extended tube caused more of an interference effect on the combined vortex core. Because of the different passive effects of the injection tubes, the quantitative data presented herein have been normalized to the vortex strength with the injection tubes in place. Thus, the results show only the effect of mass injection on the dissipation of the vortex. In Figure 13, the spanwise distribution of the concentrated trailed vorticity behind the split-flap vortex generator with no injection tubes is compared to that which is present when the various injection tubes are installed. The data are compared at a freestream velocity of 75 ft/sec. It can be seen that the vortex is not spread by the passive effect of the injection tubes but that the peak and total vorticity are reduced. Since circulation is the moment of the vorticity distribution about the centerline of the vortex and the vortex has not been spread, it must be concluded that the vortex has been dissipated passively by the turbulence generated by the injection tubes.

The effect of various amounts of mass injection on the vortex trailed from the split-flap vortex generator is visualized in Figure 14. If the visualized flow for zero mass injection is compared to that presented in Figure 11 it is noticed that the vortex flow is much more diffuse near the airfoil when the injection tube is in the flow. In Figure 14 it can be seen that for $m_i=0$ and $m_i=0.0034$ lb/sec, the swirling flow has a radial component of flow towards the center of the vortex

(representative of a stable vortex) while for mass flows of m_i=0.0061 and 0.0095 lb/sec, the remaining streamlines indicate that the residual swirling flow has a radial component of flow outward from the center of the vortex which is representative of an unstable vortex. It is noted further that for a mass flow of 0.0034 lb/sec, the centerline of the vortex appears to possess an oscillatory character which is typical of the kink-type of instability associated with jet flows. While it is believed that the visualized flows presented in Figure 14 demonstrate the vortex instability that has been sought as the most efficient means of dissipating the concentrated trailed vortex by mass injection, the wind tunnel controls were not fine enough to fully document this mode of dissipation.

In regard to the flow pictures presented in Figure 14 and those that will be presented in a later section of this report, it should be noted that at the higher values of injected flows, the injected flow velocity was sufficiently high to burst the helium-filled bubbles. Therefore, care must be taken in interpreting the flow pictures to insure that not too much is read into the effects of injected mass flow on the dissipation of the trailed vortex. More specifically, the absence of helium-bubble streaks does not necessarily indicate an increased dissipative effect of mass injection, as it may well indicate that the bubbles are being burst by the shearing action between the injected flow and the freestream.

While the visualized flow pictures presented for the split-flap vortex generator might be subject to various interpretations, the quantitative data measured in the wake of the vortex generator is more straightforward. The change in the strength of the circulation in the vortex generated by the split flap as a function of injected mass flow is presented in Figures 15 and 16 for two values of the freestream velocity. The data presented in these figures were obtained for the same included angle of attack and for the same vortex injection tubes. It is noted that while the general characteristics of the

variation of the circulation strength as a function of injected mass flow are the same at the two freestream velocities, there are significant differences in the data. The effect of the velocity of the injected mass flow relative to the freestream velocity is shown in Figures 15 and 16 by comparison of the results obtained with injection tube 2 with those obtained for tube 1. Since the cross-sectional area of tube 2 is larger than that of tube 1, the exit velocity is less for tube 2 than it is for tube 1 at the same injected mass flow. As can be seen, the higher injection velocity is more efficient in dissipating the vortex at both freestream velocities. The different efficiencies of the relative velocity correlates very well with the effect of relative velocity predicted by the theoretical formula presented in Equation (5). For a given mass flow, it is noted that the strength of the trailed vortex was reduced more at V=75 ft/sec than it was at 115 ft/sec for the same injection tube (injection tube 1). The reason for this difference was thought to be because of the vortex mixing distance behind the airfoil (Figure 11). In order to investigate this phenomenon, injection tube 1 was extended by three inches in the downstream direction (injection tube 3) to determine if the downstream location of the vortex injection tube would have a significant effect on the results. From the results presented in Figures 15 and 16 it can be seen that at the lower tunnel speed, the effect of the downstream location of vortex injection was not significant, but that a significant effect was noted at the higher tunnel velocity. It is believed that this effect is due to the absolute time period required for the individual vortices to combine into a single vortex. If it is assumed that the vortex mixing process is a function of time, then the downstream distance for the single vortex to be formed would be greater for the higher freestream velocity than it would be for the lower freestream velocity. This conclusion is somewhat substantiated when it is noted that the efficiency of vortex dissipation obtained by the extended injection tube (injection tube 3) at 115 ft/sec correlates very well with that obtained with the shorter

injection tube (injection tube 1) at the lower freestream velocity. It was concluded therefore that efficiency of vortex dissipation at the lower freestream velocity could be compared at the higher freestream velocity only if the results obtained from injection tube 1 were compared with those obtained with tube 3. In addition, since the larger injection tube (injection tube 2) was not extended in the downstream direction at V=115 ft/sec, only a qualitative comparison of the effect of injection velocity could be made at a freestream velocity of 115 ft/sec.

In order to determine the effect of the location of the injection tube relative to the center of the core of the vortex, tests were conducted with the injection tube offset 1/2 the core radius. The results that were obtained from these tests are compared with those obtained with the vortex injection tube placed at the center of the core in Figure 17. It can be seen from the results presented in Figure 17 that for a given injected mass flow the offset injection tube is less efficient than when the injection tube is aligned with the center of the vortex. While the effect of injection location was found to have about a 10% effect on the efficiency of vortex dissipation, this effect is relatively small in comparison to the effects of mass flow and velocity of injection.

On the basis of the results obtained with the split-flap vortex generator, it was determined that both the velocity and the mass flow were important parameters in regard to the efficiency of vortex dissipation, but that the velocity of injection was probably the more important of the two effects. In addition, it was found that the efficiency of the dissipative process was very dependent upon the streamwise location of injected mass flow relative to the process of vortex formation. It was found, for example, that if the vortex was injected prior to the complete formation of the vortex, the efficiency of vortex dissipation was far less than when the vortex was injected when it was completely formed. At a freestream velocity of 115 ft/sec

the tip at the 25, 50 and 75 percent chord location so that the relative efficiency of injecting the constrained vortex during its initial formation (25% chord), after a majority of the circulatory energy had been concentrated in the core (50% chord) or when the vortex separated from the lifting surface and became a free vortex (75% chord) could be evaluated. In addition to these nozzle configurations, a slotted nozzle configuration similar to that used in the initial test program conducted under ONR sponsorship (Ref. 4) was also tested to provide a basis of comparison. The visualized flow pictures for the various nozzle configurations are presented in Figures 19 through 22. The various mass flows used were the same for each nozzle so that a direct comparison can be made of the visualized flow for all configurations.

Figure 19 presents the flow pictures for the model having the injection slot at the 25% chord. When the flows for the various mass injection rates are compared, it becomes obvious that the injected flow at this chordwise location seems to spread the circulatory flow in the irrotational part of the vortex and that very little dissipative effect occurs in the vortex core. This spreading of the outer vortex flow is not evident except at an injected mass flow of 0.0093 lb/sec.

It should be noted that the increased lightened area at the tip of the model is due to the accumulation, with time, of the soap film from the burst bubbles.

Figure 20 presents flow pictures for the injection nozzle placed at the 50% chord position. It can be seen from this set of flow pictures that the outer vortex flow was not spread to the degree that it was with the nozzle at the 25% chord position. It is also apparent that the desired dissipative effect in the vortex core became more effective with increasing injected mass flow. For the maximum mass flow used, m_i=0.0146 lb/sec, no indication of a concentrated vortex remained although an overall swirl pattern, with random turbulence superimposed, remained in the near wake.

Figure 21 presents the flow pictures for the injection slot located at the 75% chord position. In comparing these flow pictures with those taken for the injection slot at the 25 or 50 percent chord position, it is obvious that this location is the most efficient, as regards vortex dissipation. For example, the dissipative process seems to become more pronounced at lower injection rates and the maximum dissipation occurring at the 50% chord position for a mass flow of m_i=0.0146 lb/sec seems to be obtained at a mass flow of m_i=0.0122 lb/sec for the injection slot at the 75% chord position.

Figure 22 presents the flow pictures for the model having an elongated chordwise slot similar to that in Reference 4. Comparison of these flow pictures with those taken for the injection slot at the 50 and 75 percent chordwise positions indicates that the effective dissipative action of the elongated slot was similar to that of the injection slot located at the 50 percent chord position and less than that of the slot located at the 75 percent chord position. Based on these results, further testing of the elongated slot was not undertaken.

Figure 23 presents the quantitative results that were obtained for the injection slots located at the different chordwise locations. It can be seen that the quantitative results bear out the qualitative evaluation made on the basis of the visualized flow, that is, the most efficient dissipative action was obtained with the injection slot located at the 75% chord. It should be noted that the visualized flow pictures were not obtained over as extensive a range of mass flows as that for which the quantitative data were obtained with a vortex meter, since for mass flows greater than 0.015 lb/sec a significant number of the bubbles were broken due to the aerodynamic shearing action, and thus the benefits of mass injection might be interpreted to be more beneficial than that actually achieved.

In order to determine the effect of angle of injection on the efficiency of vortex dissipation, the model was tested with the angle of injection 5 degrees less than the angle at which

the trailed vortex left the lifting surface. These results are compared to those obtained with the angle of injection equal to the angle of attack in Figure 24. While there is some scatter in the data, the data for the injection angle less than the angle of attack shows that this injection process is not as efficient as regards vortex dissipation in comparison to that with the injection angle equal to the angle of attack.

While the tests of the various injection slots indicated that the 75% chord position was the most efficient as regards vortex dissipation, the results also indicated that the efficiency of three-dimensional injection slots was not comparable to that obtained with the injection tubes used during the split-flap tests. Figure 25 compares results obtained during the split-flap tests with those obtained with the slotted nozzles on the three-dimensional lifting surface.

These data obtained for a circulation strength of about the same magnitude indicate the far greater effectiveness of the injection tube. It was rationalized that this large difference could be either due to the difference in the injection velocity or due to the fact that the injection tubes injected air directly into the core and the slots had to inject the air through the vortex first before the air was entrained in and along the axis of the vortex core. To investigate these two possibilities, a circular nozzle was constructed such that it was centered at the 75% chordline and also so that different length and diameter tubes could be inserted to change the injection velocity or the streamwise location at which the vortex was injected. Figures 26 through 30 present visualized flow pictures of the various configurations that were tested.

Figure 26 presents the flow pictures of the 1/4-inch diameter nozzle with no extension tube. When these flow pictures are compared to those in Figure 21 for the slotted nozzle, it is seen that roughly the same dissipative action was achieved with about one-half the mass flow. The basic difference between these configurations was the velocity of injection which was higher for the circular nozzle.

Figure 27 presents the flow pictures for a short 3/16-inch I.D. tube inserted in the 1/4-inch nozzle and Figure 28 shows the flow pattern for a longer 3/16-inch tube. In comparing the various sets of flow pictures it can be seen that the 3/16-inch short tube was much more effective than the 1/4-inch round nozzle probably because of the higher injection velocity and also because the extended tube apparently caused some separation which in turn resulted in additional dissipation due to turbulence. As the injection velocity was increased further by using a 1/8-inch I.D. tube (Figure 29) the vortex dissipation process was enhanced further but again the tube extension was noted to create some additional turbulence (Figure 30). Further increase of the injection velocity was not attempted as the injected velocity for the 1/8-inch tube was close to sonic.

Figure 31 presents a comparison of the quantitative results obtained with the short tube nozzles at the tip of the lifting surface. The quantitative data indicate an effect essentially the same as that deduced from the flow pictures, that is, the higher the injection velocity, the more efficient the dissipation of the concentrated vortex.

C. Comparison of Theoretical and Experimental Results

The inductive theory presented in an earlier section of this report was used to predict the effect of mass injection on the dissipation of the tip vortex for the model configuration tested during this program and those tested in Reference 4, and 10. The theoretical results are compared with the experimental results in Figure 32. It can be seen that the correlation is excellent although the range of test conditions and model parameters is rather extensive. It is noted that for the split-flap airfoil tests, the radius of the core is larger than it is for the various three-dimensional models. This larger value of the core radius is consistent with the higher drag of the split-flap configuration.

It is noted that the theoretical curves indicate that as mass flow is applied, no dissipative action is predicted until a given mass flow is achieved and then a very rapid dissipative

action suddenly occurs as the mass flow is increased further. This break point in the theoretical curve is associated with the velocity of injection relative to the freestream or the axial velocity in the core of the vortex.

It is believed that the theory in its present form, can be used to obtain a reasonable estimate of the effect of injected mass flow on the dissipation of a concentrated trailed vortex of a given strength and size. However, since the theory cannot predict the stability characteristics of swirling flow mixing with a highly turbulent viscous jet, it cannot be used to determine the possible additional beneficial effects as regards the rapid dissipation of the vortex that might be obtained by triggering the inherent flow instability which exists in such flows.

V. CONCLUSIONS AND RECOMMENDATIONS

On the basis of the research that was conducted it was concluded that the concentrated trailed tip vortex from a three-dimensional lifting surface can be readily dissipated by mass injection far more efficiently than had been previously demonstrated. It is believed that this technique of vortex dissipation is a very practical solution of eliminating the detrimental effects of a concentrated vortex trailed from either a helicopter blade or a fixed-wing aircraft since the dissipative action occurs downstream and does not degrade the flow over the airfoil. On the basis of the experimental results, a theory of progressive vortex dissipation was developed which, given the initial characteristics of the vortex, predicts the change in the vortex strength with mass injection as it moves in a downstream direction. The applicability of the theory has been demonstrated by comparison of the predicted results with experimental results which cover an extensive range of test conditions and model parameters.

In addition to the above general conclusions the following specific conclusions are also noted.

1. Both mass flow and velocity of injection are important parameters as regards the efficiency of dissipation.
2. To maximize the efficiency of dissipation, the injection velocity should be maximized and thus a sonic nozzle should be used.
3. The high pressure ratios required to attain the high velocities of injection precludes the application of centrifugal pumping as a method for vortex dissipation.
4. Injection of the vortex prior to its complete formation significantly reduces the dissipative effect of mass injection.

5. The 75% chord position is the most beneficial location for injecting the tip vortex generated by a three-dimensional lifting surface.

6. The most efficient manner of injecting the vortex is at its center and parallel to the centerline of the trailed vortex.

7. Because of the pressure ratios required to maximize the efficiency of the vortex injection system, the application of this dissipation technique to a circulation-controlled airfoil would probably require a system separate from that used for circulation control.

On the basis of the results obtained in this research program, it is recommended that the following tasks be undertaken as soon as possible so that full-scale production applications to helicopters and fixed-wing aircraft can be made.

For Helicopters

1. Determine the effect of transonic tip speeds on the effectiveness of the technique.

2. Determine the effect of effective sweep due to forward flight on the vortex formation and the requirements of the injection system.

3. Modify a full-scale rotor system and test the effectiveness of the technique in reducing the dynamic loads and the acoustic output in various flight regimes.

For Fixed-Wing Aircraft

1. Determine the manner by which the vortex forms and trails from the wing-flap juncture and test the effectiveness of the mass injection technique in dissipating this concentrated vortex.

2. Apply and test the technique of mass injection to the flap and wing tip of a full-scale aircraft.

VI. REFERENCES

1. Air Force Office of Scientific Research and the Boeing Scientific Research Laboratories. "Aircraft Wake Turbulence Symposium", Seattle, Wash., September 1-2-3, 1970.

2. Federal Aviation Administration. "Symposium on Turbulence", Washington, D.C., March 22-23-24, 1971.

3. Rinehart, Stephen. "Study of Modification of Rotor Tip Vortex by Aerodynamic Means", ONR Contract N00014-69-C-0169, Rochester Applied Science Associates, Inc., RASA Report No. 70-02, AD 704804, 1970.

4. Rinehart, S.A., Balcerak, J.C., White, R.P., Jr. "An Experimental Study of Tip Vortex Modification by Mass Flow Injection", ONR Contract N00014-69-C-0169, Rochester Applied Science Associates, Inc., RASA Report No. 71-01, AD 726736, 1971.

5. Schlichting, Hermann. Boundary Layer Theory, McGraw-Hill Book Company, 4th Edition, 1960, pp. 607-608.

6. Batchelor, G.K. "Axial Flow in Trailing Line Vortices", Journal of Fluid Mechanics (1964), Vol. 20 Part 4, pp. 645-658.

7. Hornbeck, R.W. "Viscous Flow in a Short Cylindrical Vortex Chamber With a Finite Swirl Ratio", Lewis Research Center, NASA Report No. TN D-5132, Nov. 27, 1968.

8. Savino, J.M. and Keshock, E.G. "Experimental Profiles of Velocity Components and Radial Pressure Distributions in a Vortex Contained in a Short Cylindrical Chamber, NASA TN D-3072, 1965.

9. Chigier, N.A. and Corsiglia, V.R. "Tip Vortices - Velocity Distributions", AHS Preprint #522, Presented at the 27th Annual National Forum of the American Helicopter Society, Washington, D.C., May 19-21, 1971.

10. White, R.P., Jr., and Balcerak, J.C. "Investigation of the Dissipation of the Tip Vortex of a Rotor Blade by Mass Injection", U. S. Army Air Mobility Research & Development Laboratory, Ft. Eustis, Va., Contract No. DAAJ02-71-C-0036, Rochester Applied Science Associates, Inc., RASA Report No. 72-03, 1972.

11. Williams, Robert M., and Howe, Harvey J. "Two-Dimensional Subsonic Wind Tunnel Tests on a 20-Percent Thick, 5-Percent Cambered Circulation Control Airfoil", NSRDC Tech Note AL-176, August 1970.

12. Englar, Robert J. "Two-Dimensional Transonic Wind Tunnel Tests of Three 15-Percent Thick Circulation-Control Airfoils", NSRDC TN AL-182, December 1970.

13. Yuan, S.W., Westkaemper, J.C., and Kishi, J.S. "Research on Elliptical Airfoil With Jet Circulation Control", ONR Aeronautics, Code 461, January 1969 (Contract N00014-68-A-0126), AD 697-179.

14. Chigier, N.A. and Corsiglia, V.R. "Tip Vortices - Velocity Distributions", AHS Preprint #522, Presented at the 27th Annual National Forum of the American Helicopter Society, Washington, D.C., May 19-21, 1971.

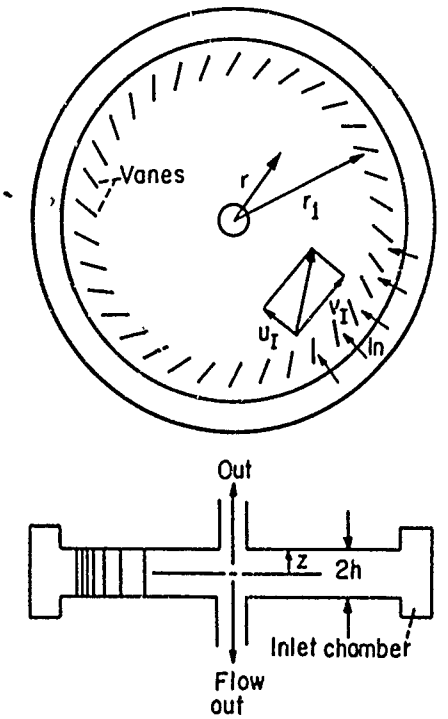

Figure 1. Typical Short-Vortex Chamber Configuration.

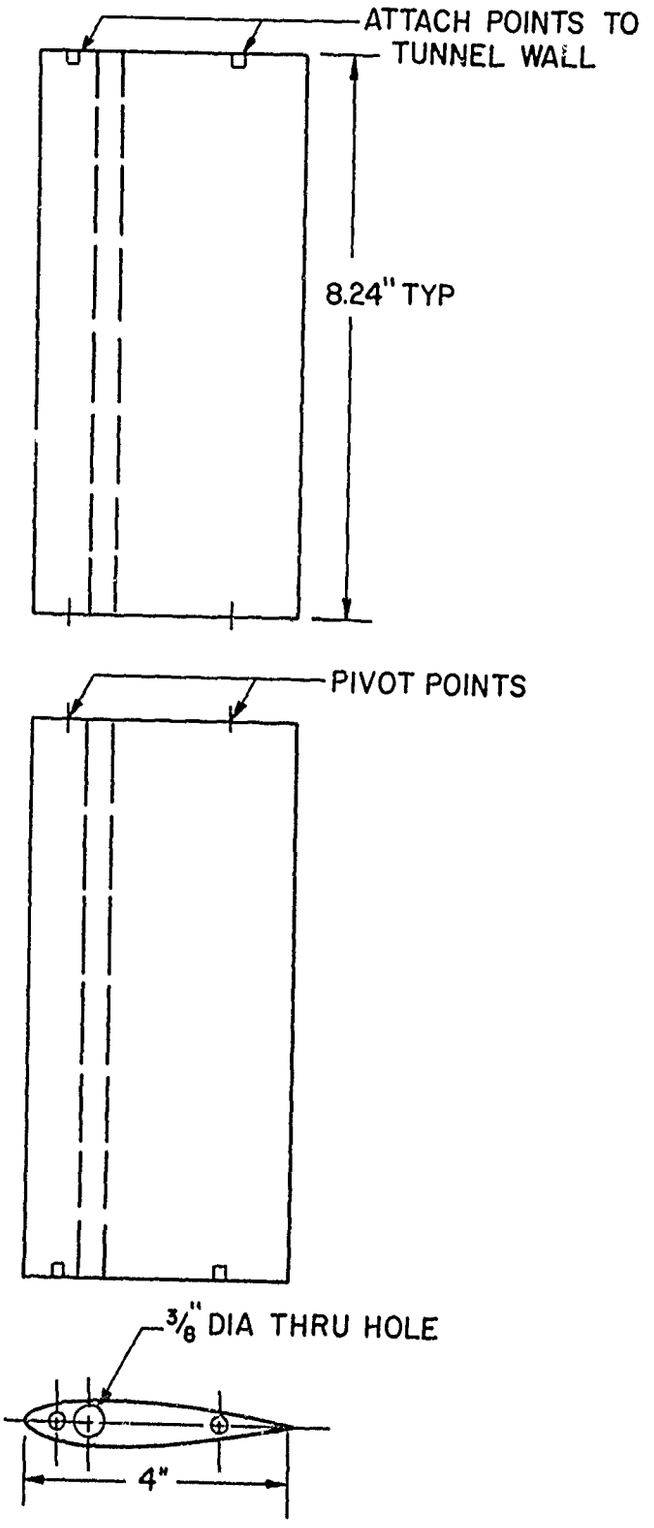

Figure 2. Schematic Diagram of Split-Flap Model Configuration.

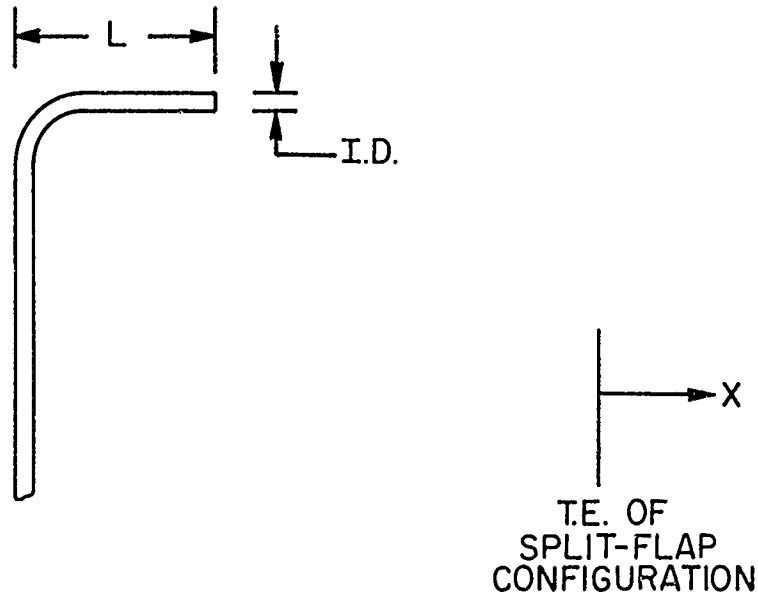

TUBE NO.	I.D. (in.)	L (in.)	X (in.)
1	0.101	1.0	-0.2
2	0.167	1.0	-0.2
3	0.101	4.0	3.8

Figure 3. Injection Tube Data for Split-Flap Tests.

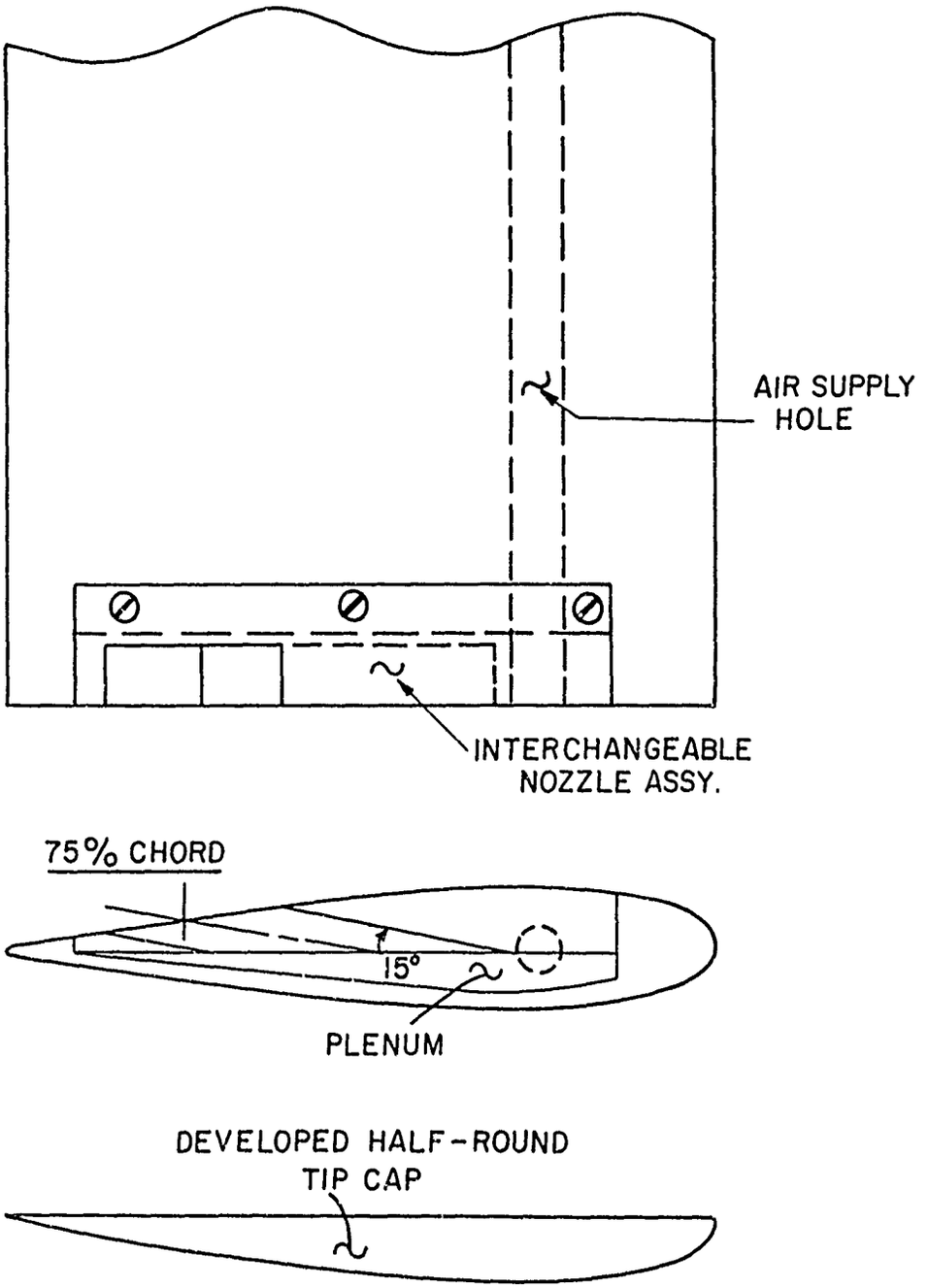

Figure 4. Schematic Diagram of Single-Airfoil Model With a Typical Nozzle Configuration.

Figure 5. Exploded View of Model and Nozzles Used in Single-Airfoil Tests.

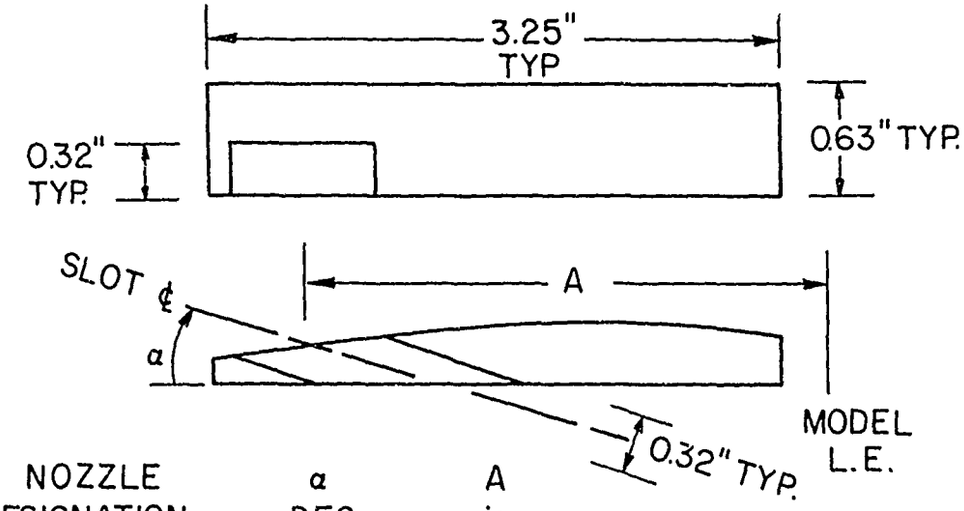

NOZZLE DESIGNATION	α DEG	A in.
25 – 15	15	1.0
50 – 10	10	2.0
50 – 15	15	2.0
75 – 10	10	3.0
75 – 15	15	3.0

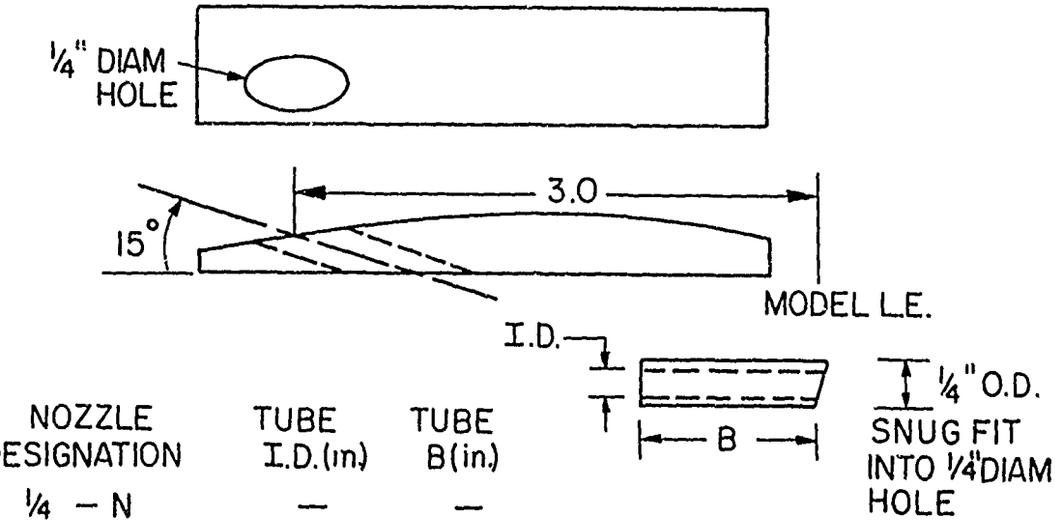

NOZZLE DESIGNATION	TUBE I.D.(in.)	TUBE B(in.)
1/4 – N	—	—
3/16 – S	3/16	1.0
3/16 – L	3/16	1.5
1/8 – S	1/8	1.0
1/8 – L	1/8	1.5

Figure 6. Nozzle Data for Single-Airfoil Tests.

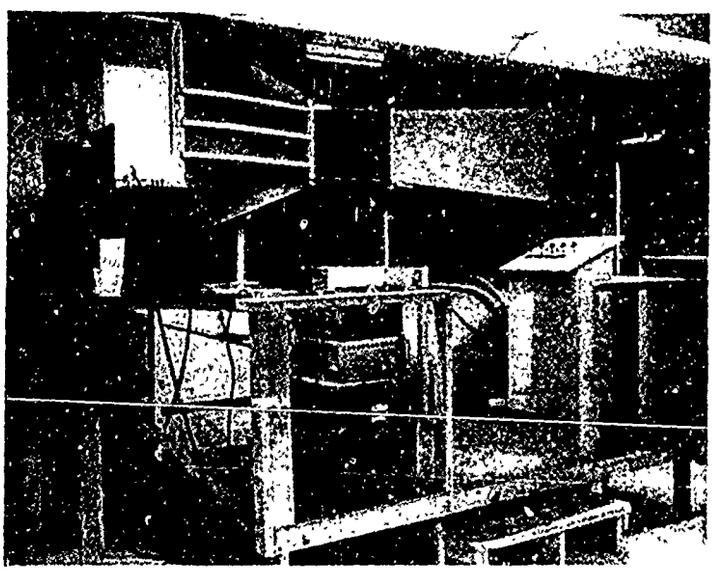

Figure 7. Installation of Model and Instrumentation for Wind Tunnel Tests.

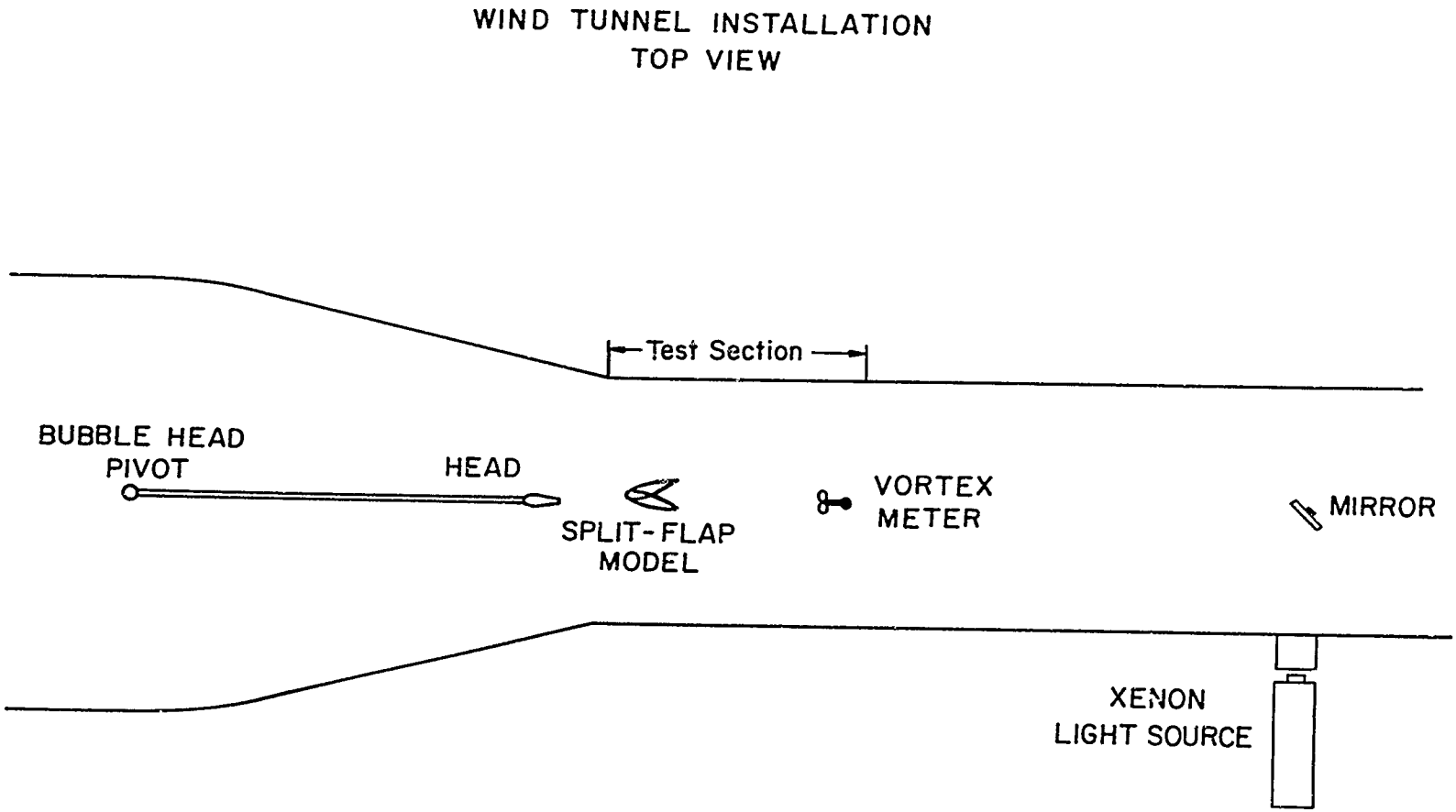

Figure 8. Schematic Diagram of Wind Tunnel Installation.

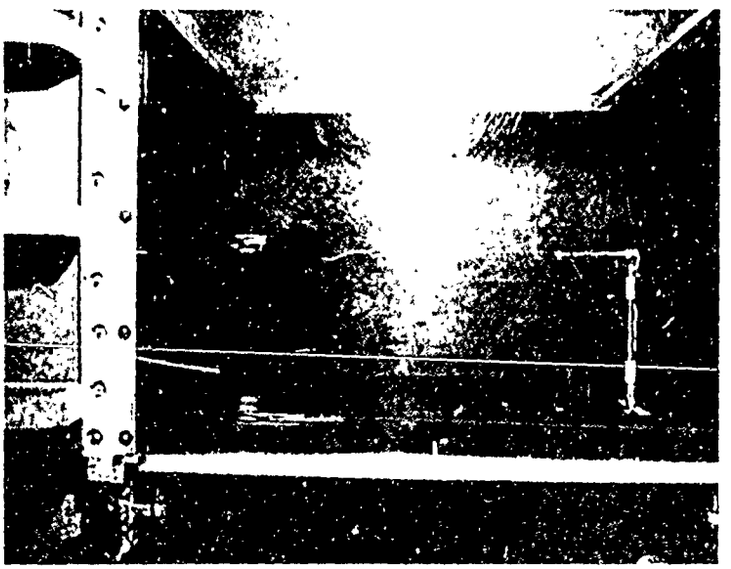

Figure 9. Installation of Model and Vortex Meter.

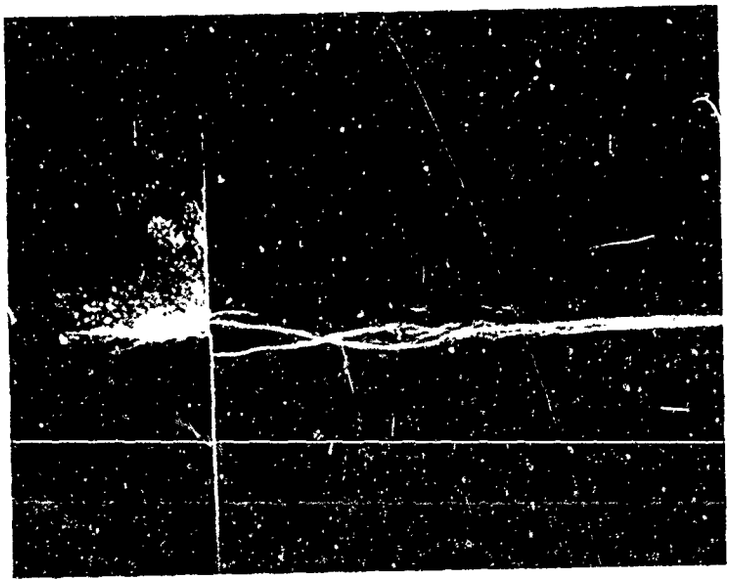

Figure 10. Vortex Formation of Split-Flap Configuration Pitched About the 75 Percent Chord.

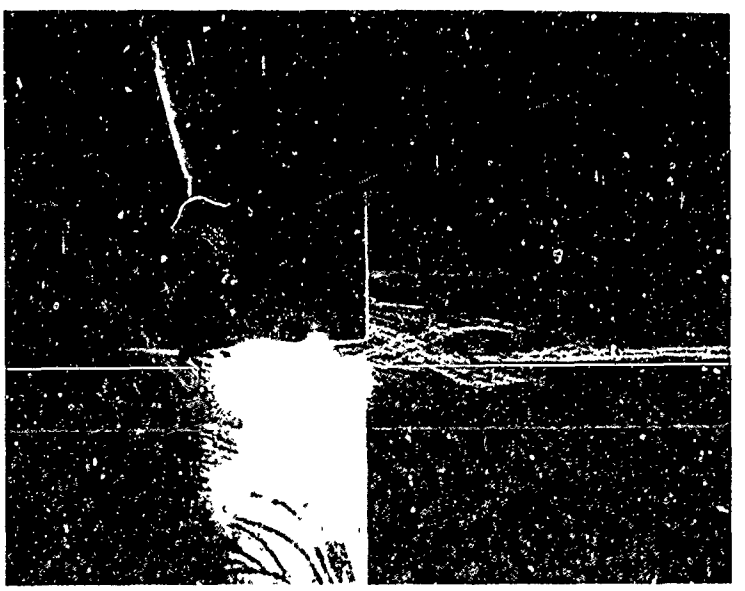

Figure 11. Vortex Formation of Split-Flap Configuration Pitched About the 12.5 Percent Chord.

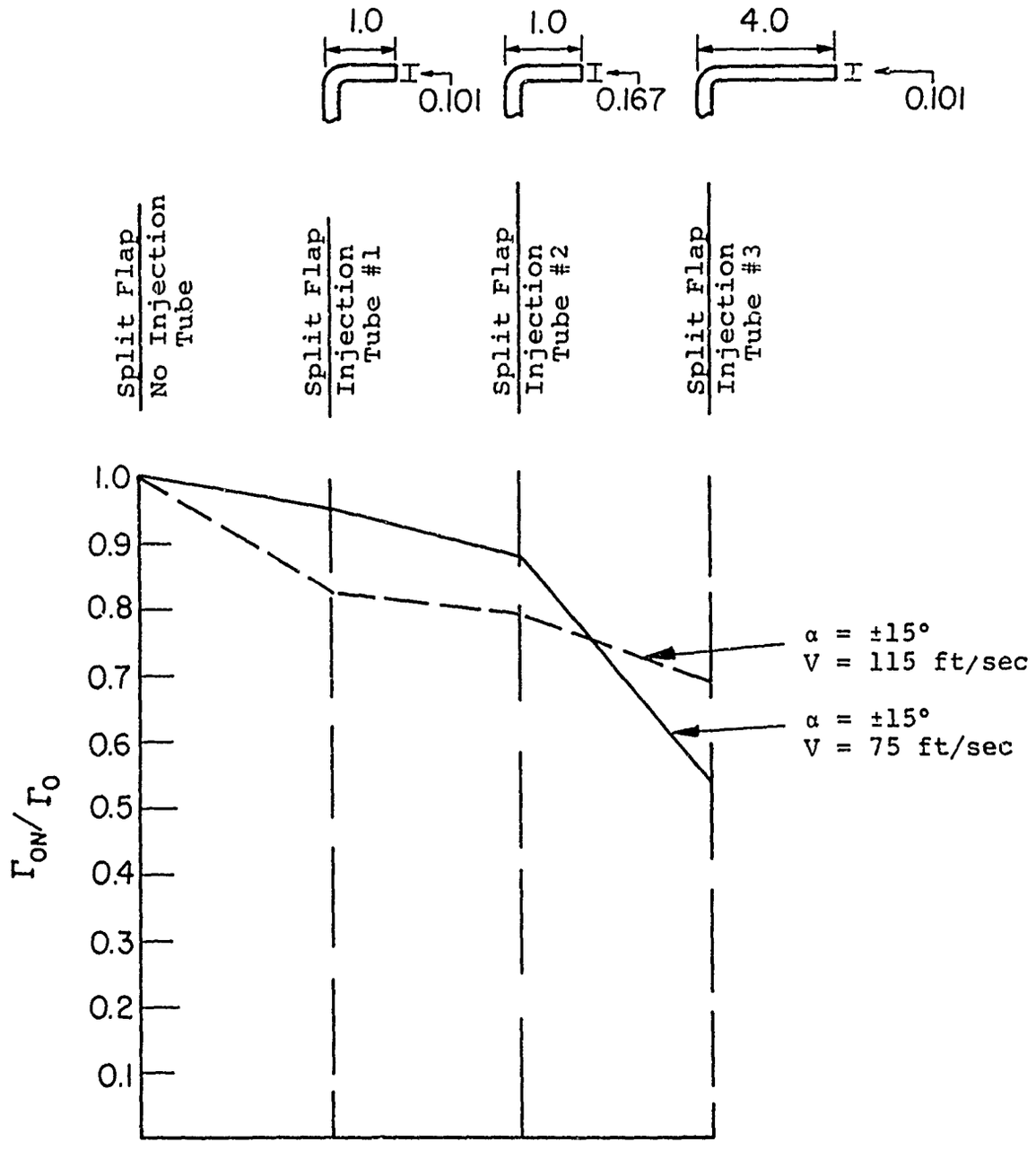

Figure 12. Passive Effect of Injection Tubes on Circulation Strength of Split Flaps.

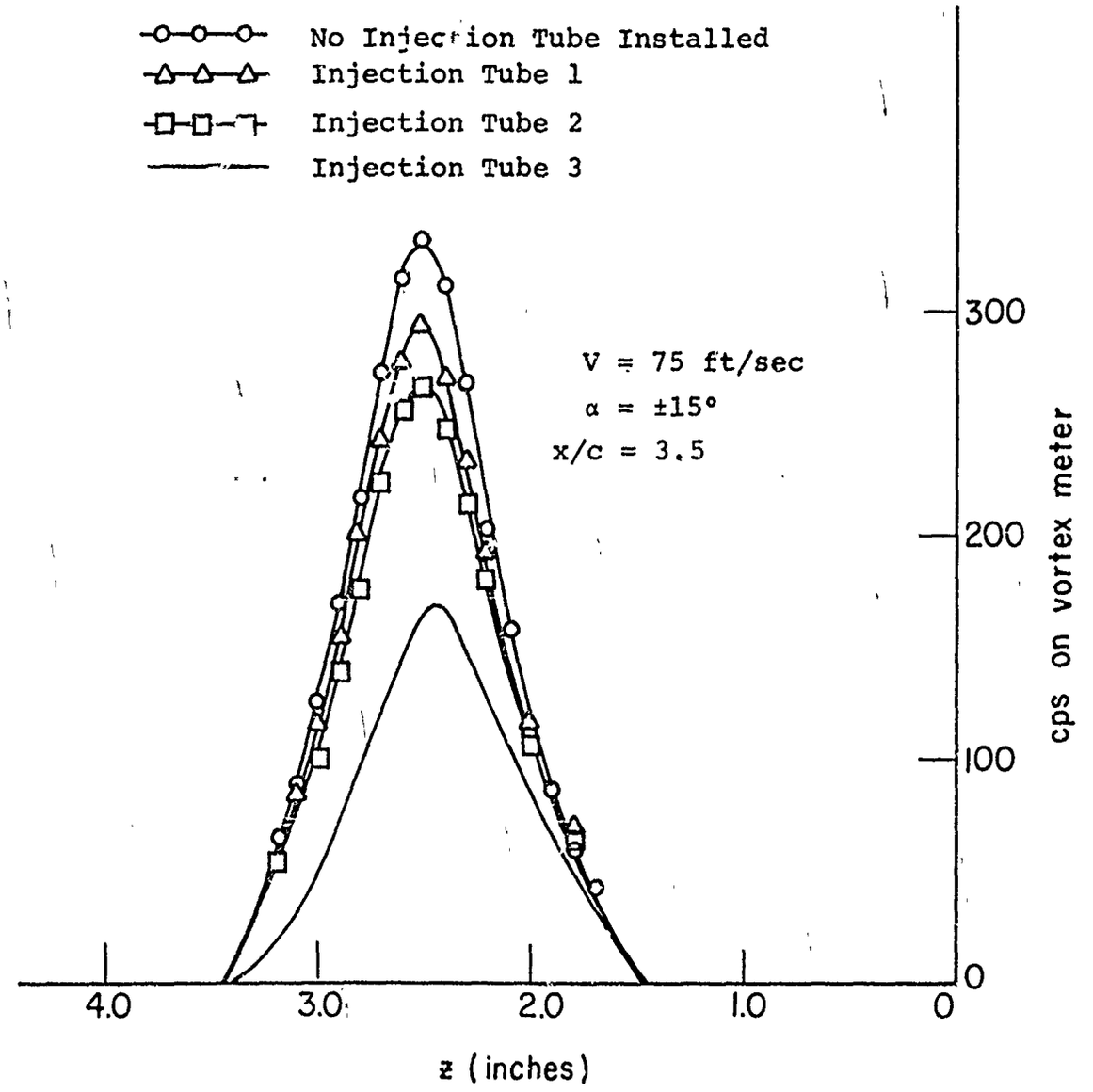

Figure 13. Vorticity Distributions of Split-Flap Configuration With and Without Injection Tubes.

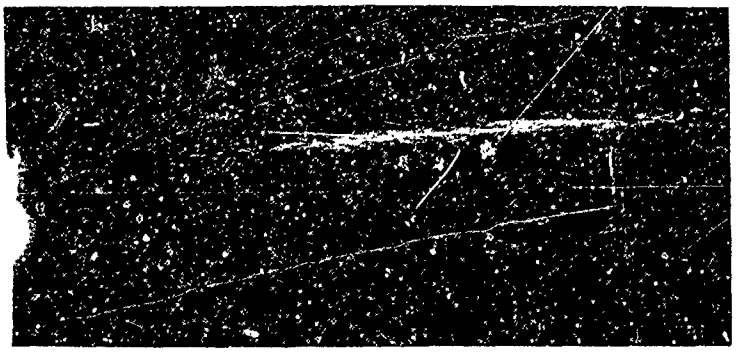

$m_i = 0$

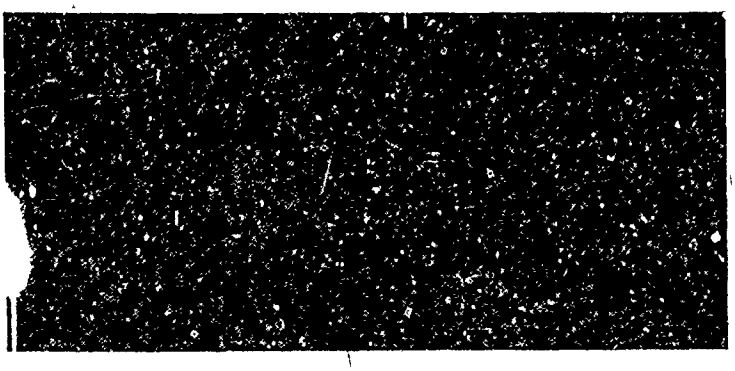

$m_i = 0.0034$ lb/sec

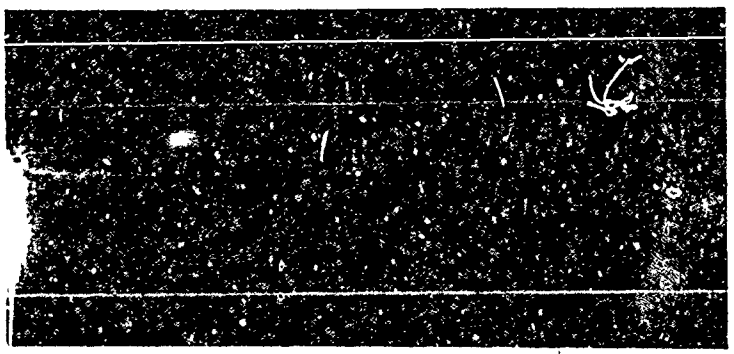

$m_i = 0.0061$ lb/sec

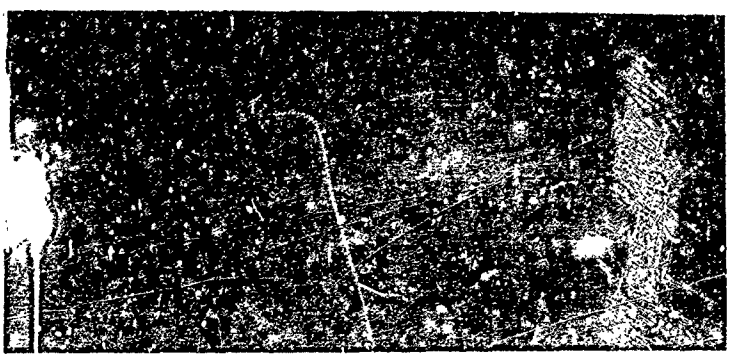

$m_i = 0.0095$ lb/sec

Figure 14. Variation of the Flow Field in the Wake of the Split-Flap Configuration With Various Amounts of Injected Mass Flow (V=75 ft/sec, $\alpha = \pm 12°$).

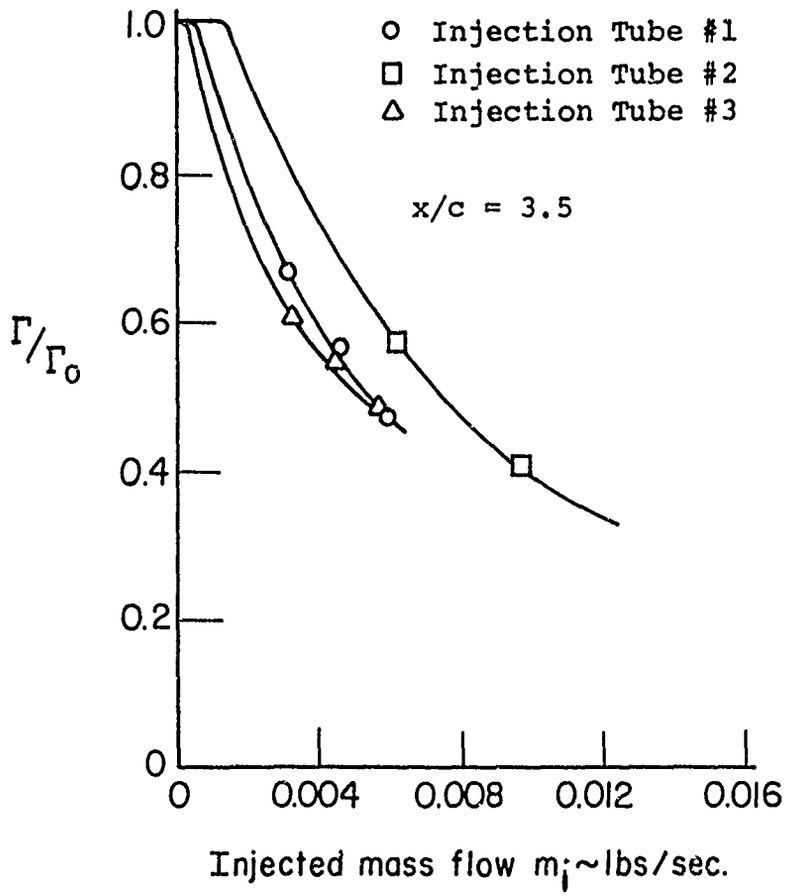

Figure 15. Γ/Γ_0 Versus Injected Mass Flow for Various Injection Tubes - V=75 ft/sec; $\alpha=\pm15°$ (Split-Flap Vortex Generator).

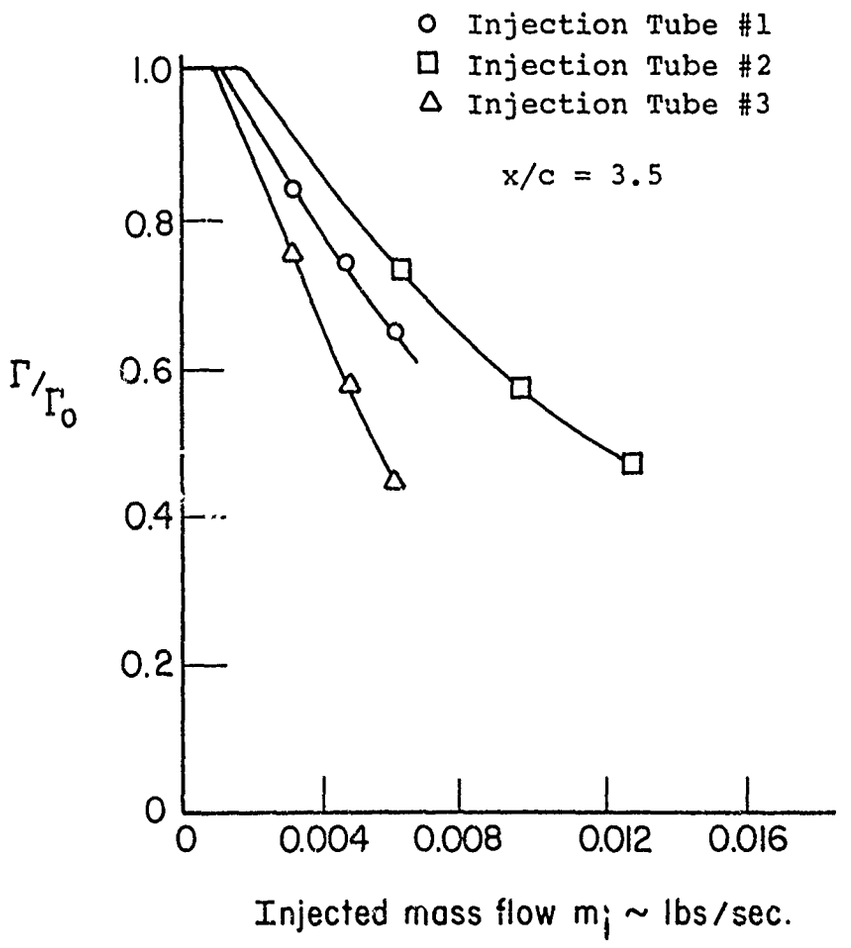

Figure 16. Γ/Γ_0 Versus Injected Mass Flow for Various Injection Tubes - V=115 ft/sec; α=±15° (Split-Flap Vortex Generator).

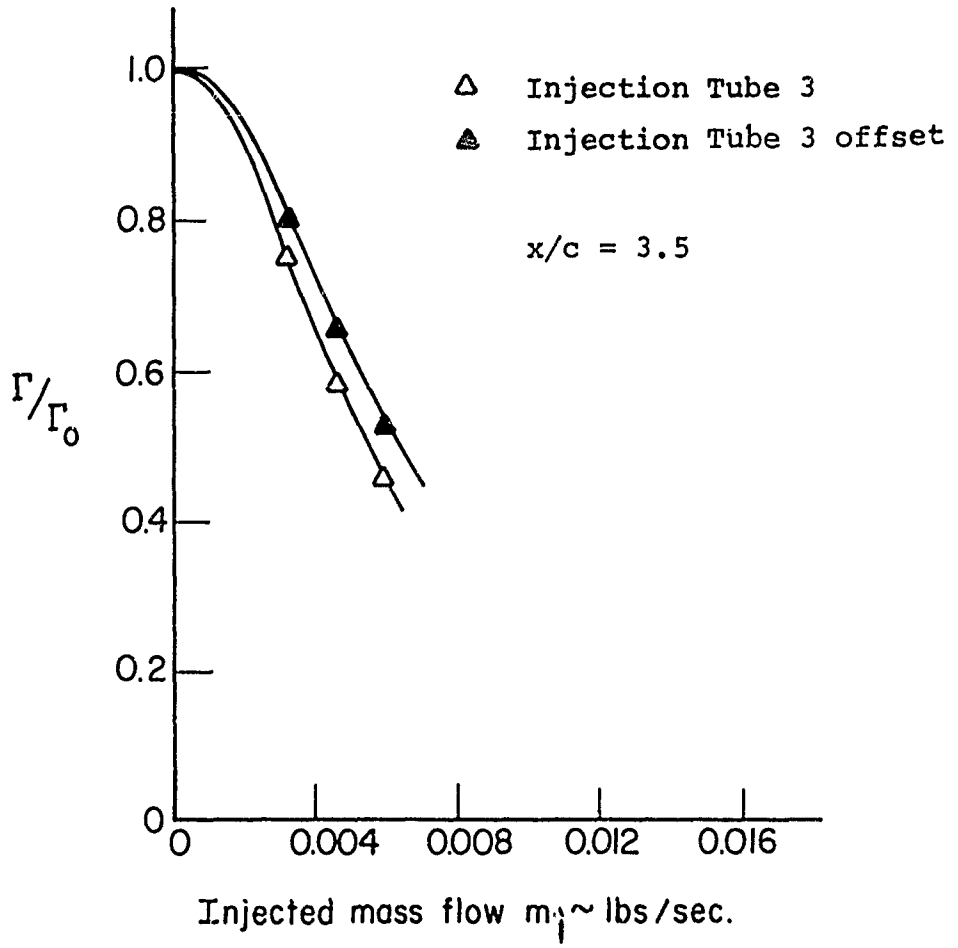

Figure 17. Γ/Γ_0 Versus Injected Mass Flow for Different Locations of the Injection Tube in the Vortex Core - V=75 ft/sec; $\alpha=\pm 15°$ (Split-Flap Vortex Generator).

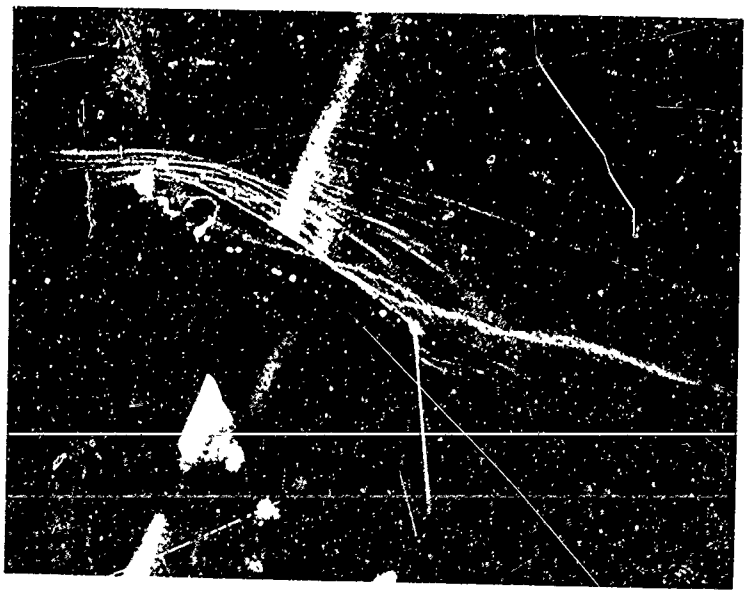

Figure 18. Vortex Formation Over Tip Section of Square-Tip Configuration; V=75 ft/sec, α=15°.

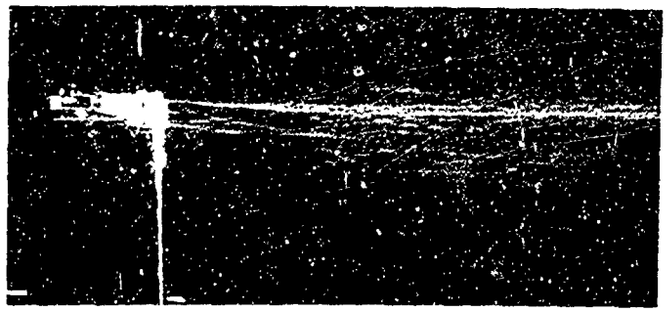

$m_i = 0$

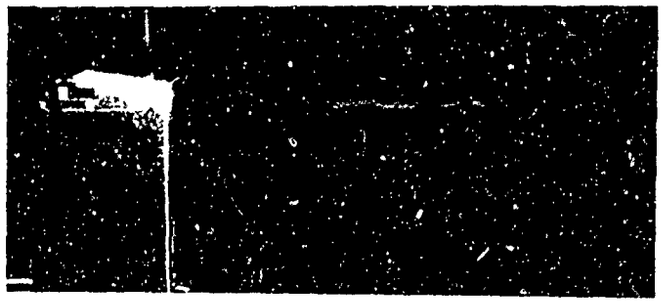

$m_i = 0.0093$ lb/sec

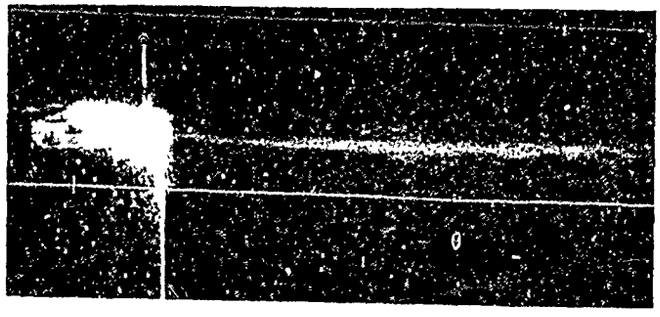

$m_i = 0.0122$ lb/sec

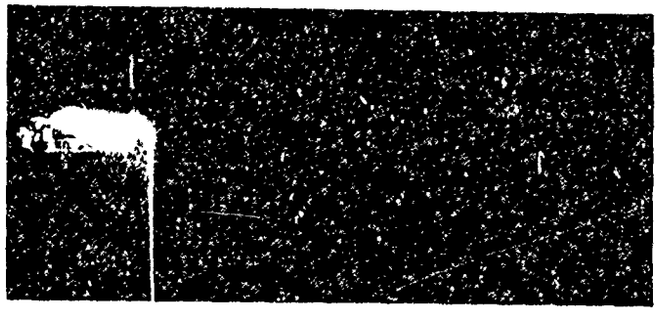

$m_i = 0.0146$ lb/sec

Figure 19. Change in the Trailed Vortex With Mass Injection; 25-15 Nozzle; V=75 ft/sec; α=15°.

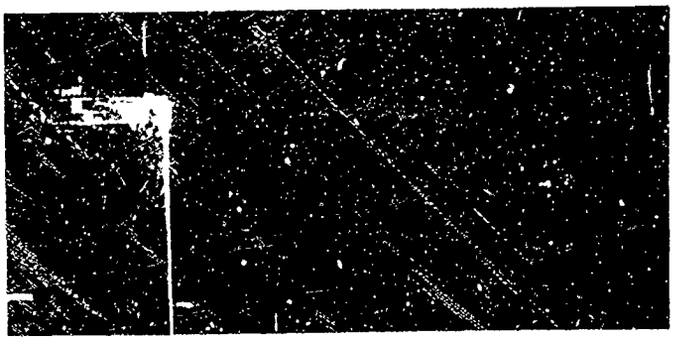

$m_i = 0$

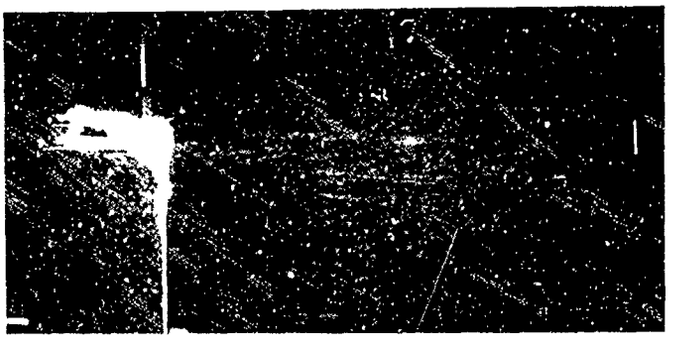

$m_i = 0.0093$ lb/sec

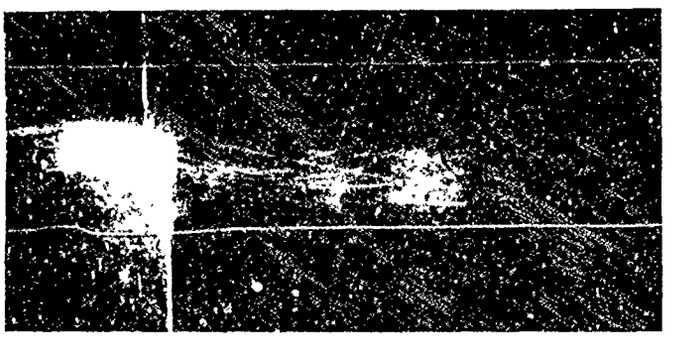

$m_i = 0.0122$ lb/sec

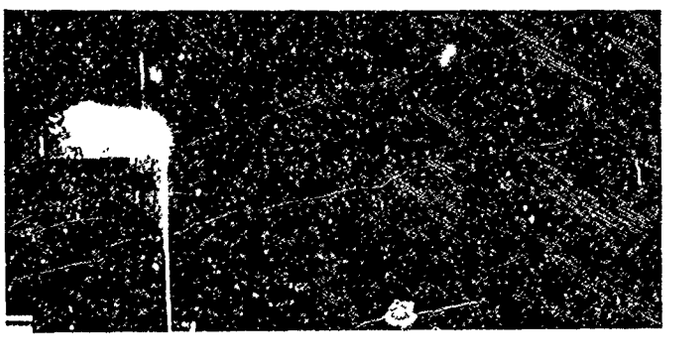

$m_i = 0.0146$ lb/sec

Figure 20. Change in the Trailed Vortex With Mass Injection; 50-15 Nozzle; V=75 ft/sec; α=15°.

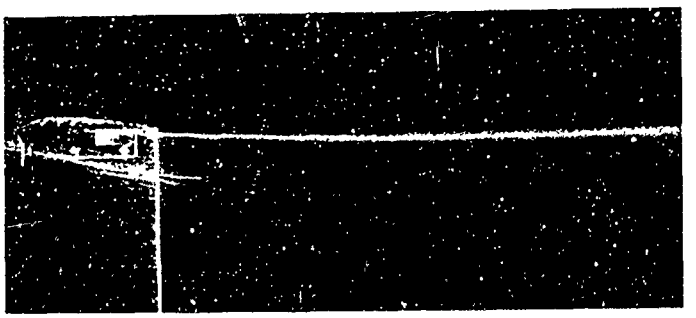

$m_i = 0$

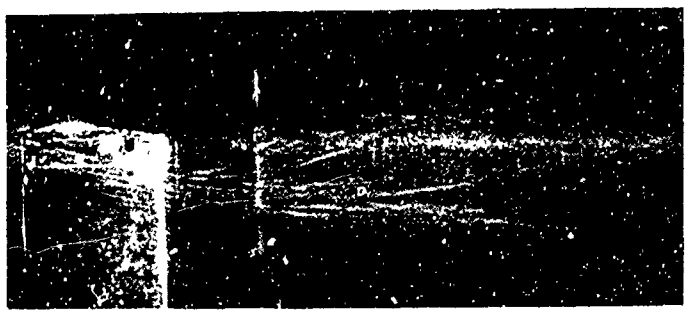

$m_i = 0.0093$ lb/sec

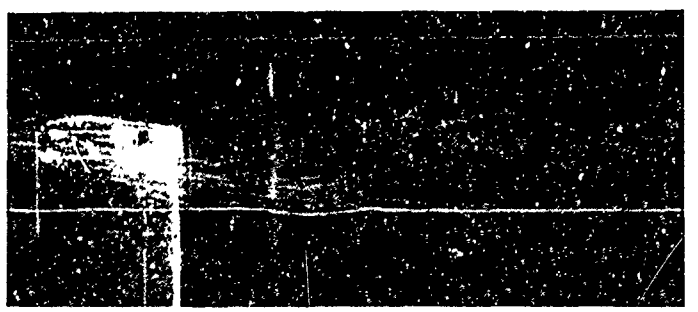

$m_i = 0.0122$ lb/sec

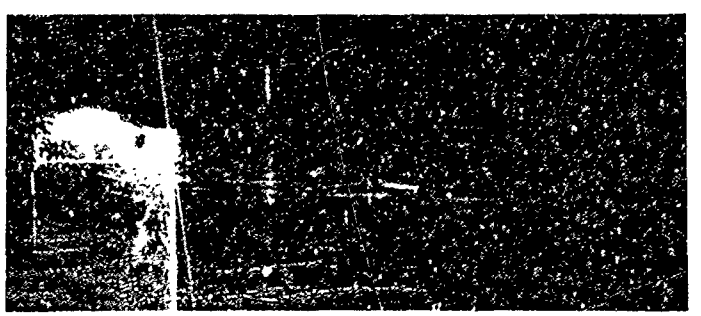

$m_i = 0.0146$ lb/sec

Figure 21. Change in the Trailed Vortex With Mass Injection; Nozzle 75-15; V=75 ft/sec; α=15°.

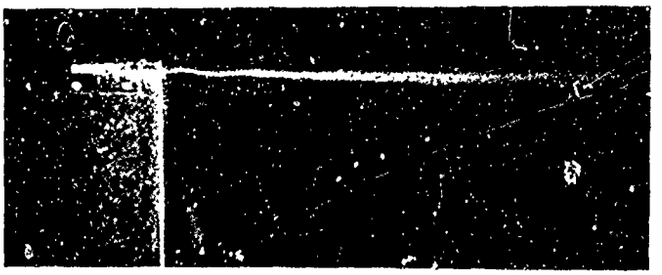

$m_i = 0$

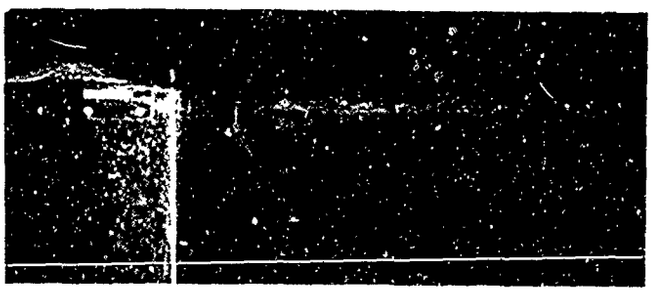

$m_i = 0.0093$ lb/sec

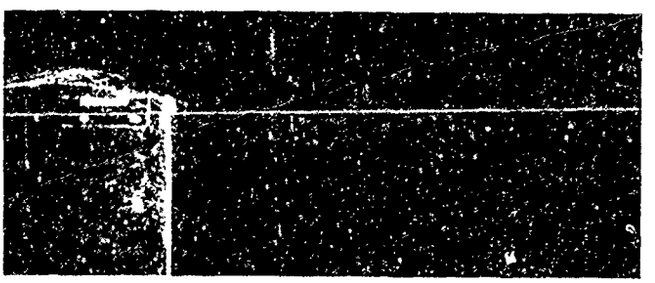

$m_i = 0.0122$ lb/sec

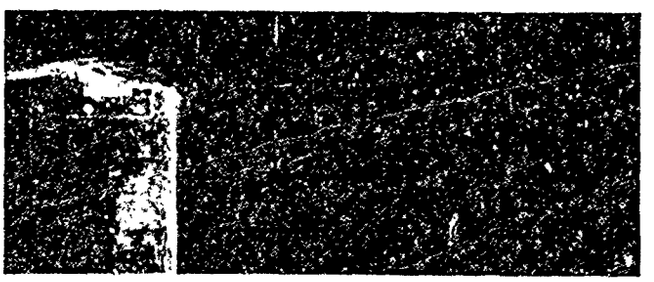

$m_i = 0.0146$ lb/sec

Figure 22. Change in the Trailed Vortex With Mass Injection; 75-15 Narrow-Slot Nozzle; V=75 ft/sec; α=15°.

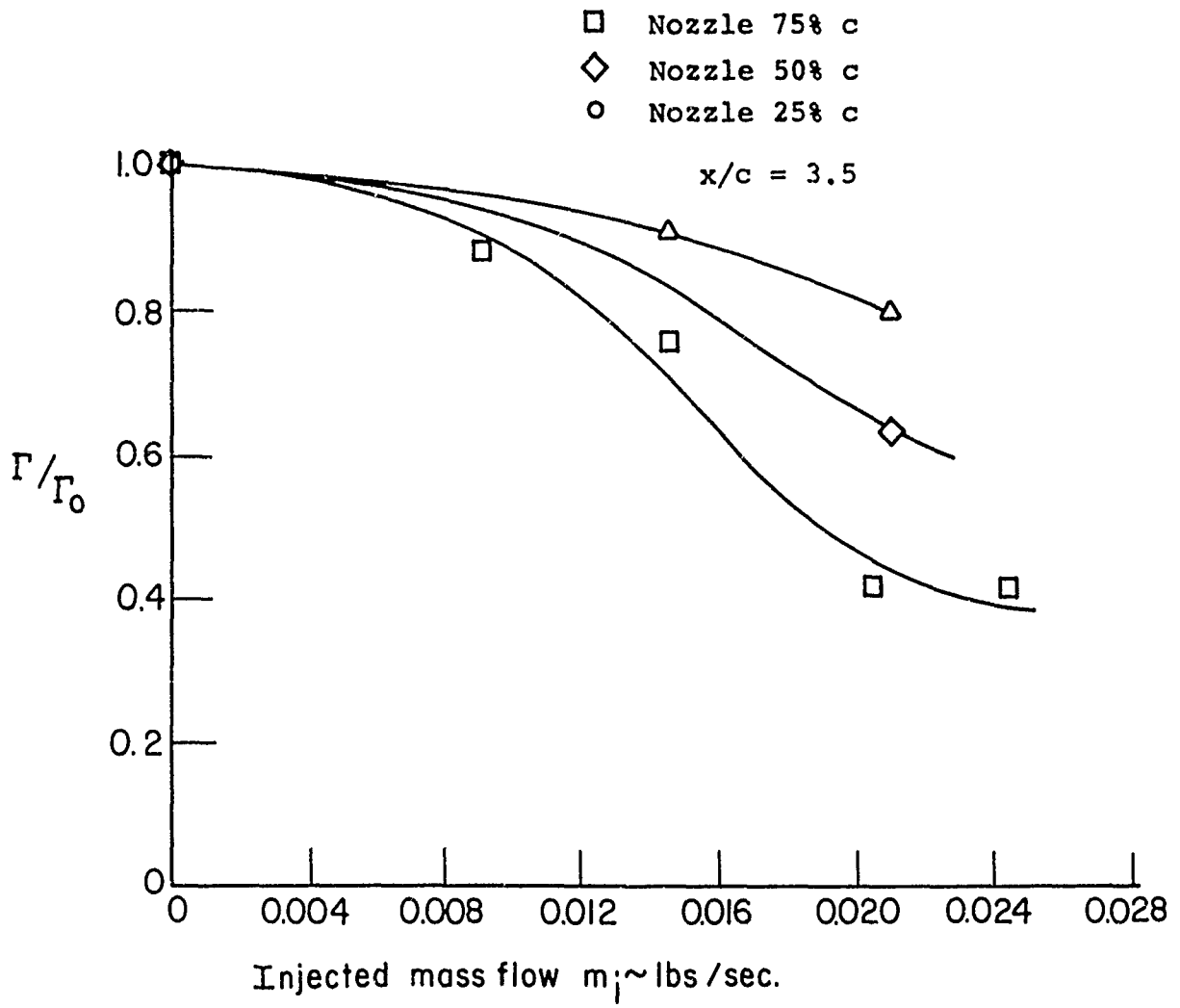

Figure 23. Γ/Γ_0 Versus Injected Mass Flow for Various Chordwise Locations of the Injection Nozzle; V=75 ft/sec; α=15° (Three-Dimensional Lifting Surface).

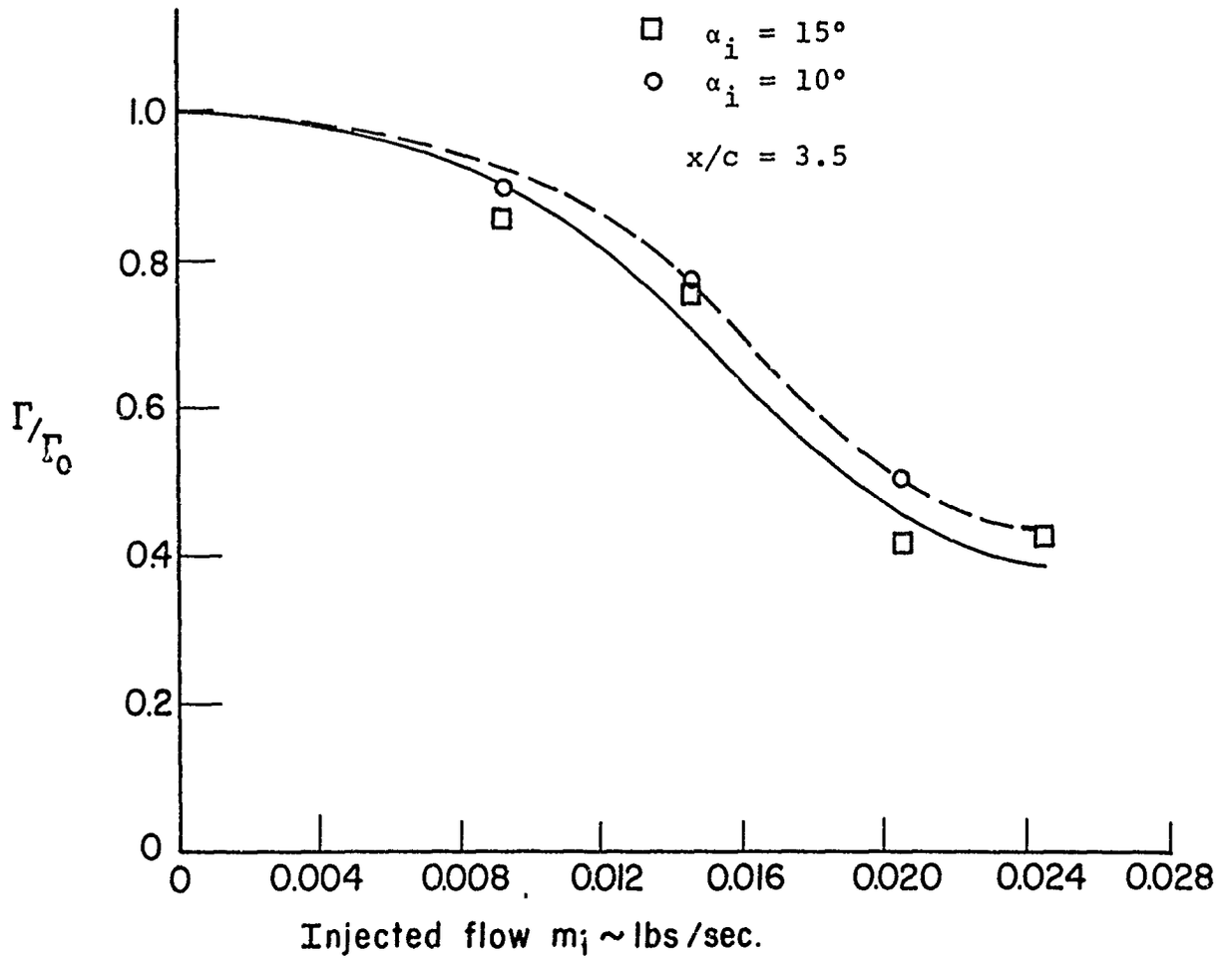

Figure 24. Γ/Γ_0 Versus Injected Mass Flow for Different Angles of Injection; V=75 ft/sec; α=15° (Three-Dimensional Lifting Surface).

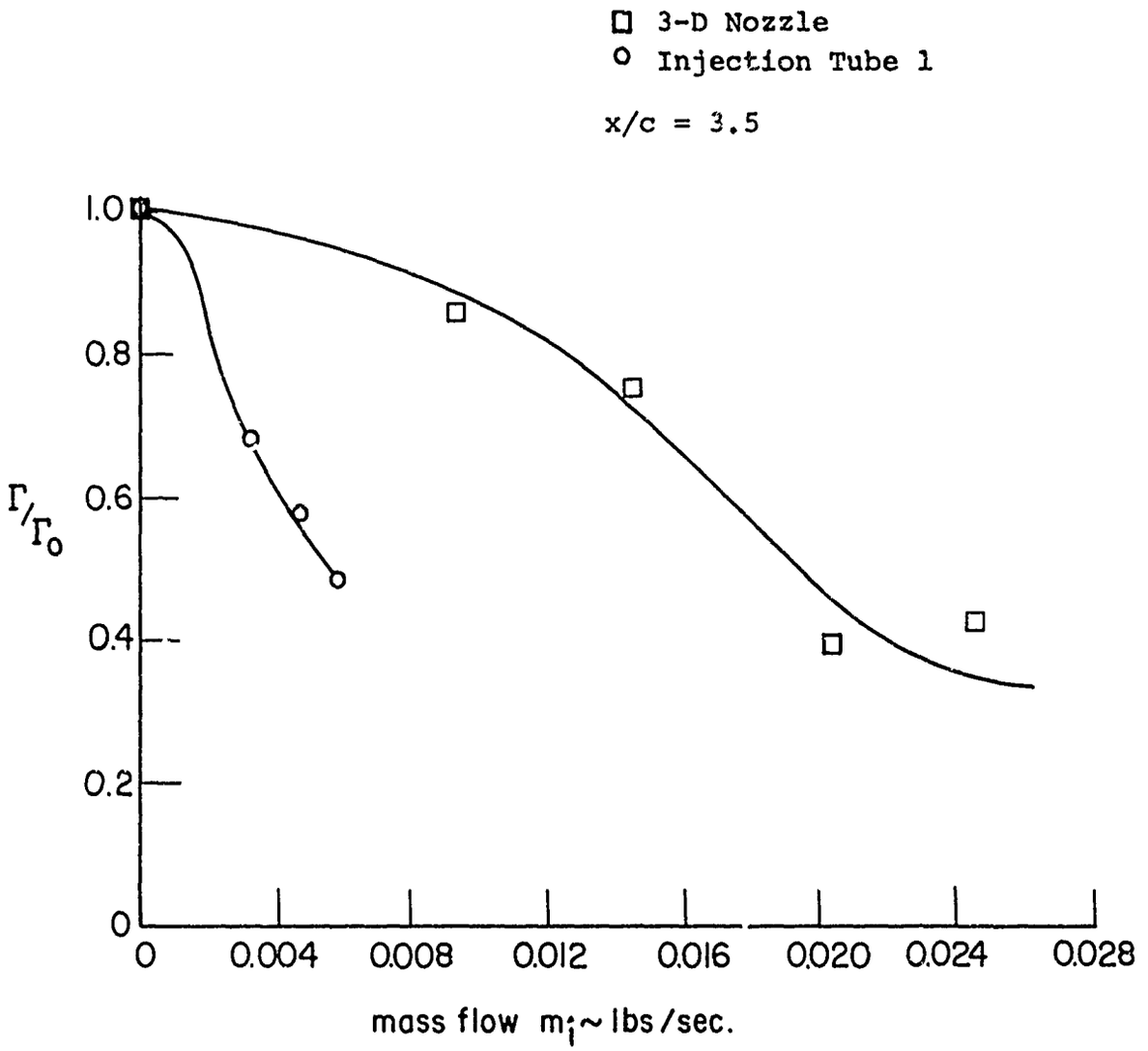

Figure 25. Comparison of Γ/Γ_0 Versus Injected Mass Flow of Three-Dimensional Slotted Nozzle With Injection Tube of Split-Flap (V=75 ft/sec; $\alpha=\pm 15°$).

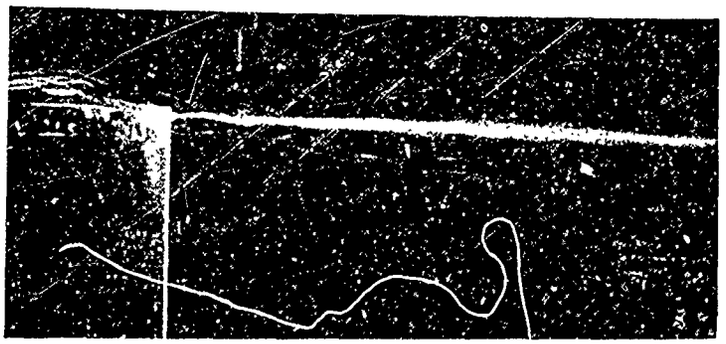

$m_i = 0$

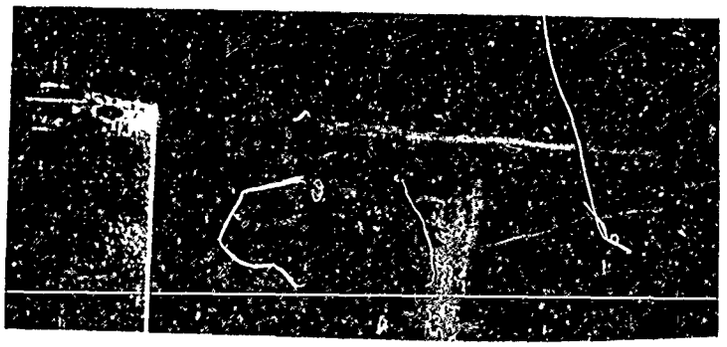

$m_i = 0.0037$ lb/sec

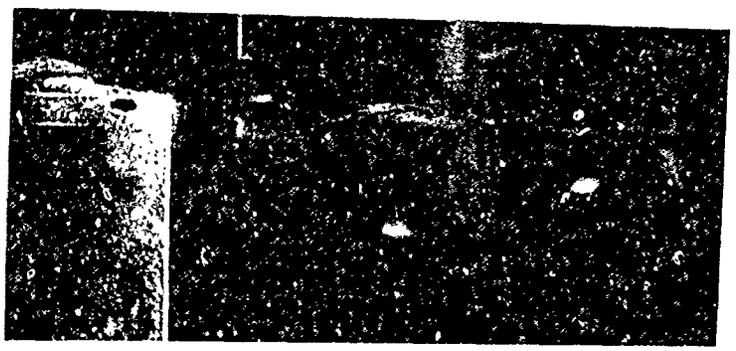

$m_i = 0.0049$ lb/sec

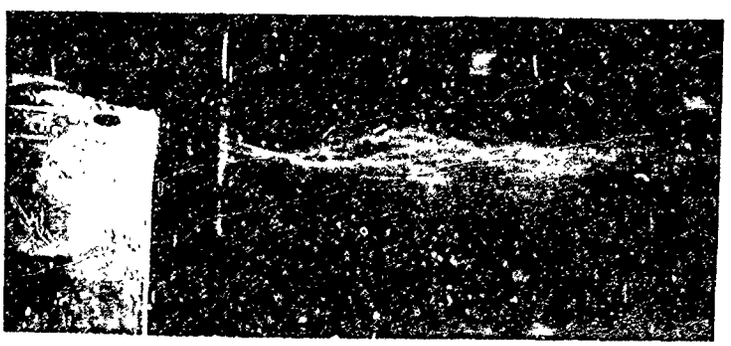

$m_i = 0.0060$ lb/sec

Figure 26. Change in the Trailed Vortex With Mass Injection; 1/4-N Nozzle; V=75 ft/sec; α=15°.

$m_i = 0$

$m_i = 0.0027$ lb/sec

$m_i = 0.0037$ lb/sec

$m_i = 0.0046$ lb/sec

Figure 27. Change in the Trailed Vortex With Mass Injection; 3/16-S Nozzle; V=75 ft/sec; δ=15°

$m_i = 0$

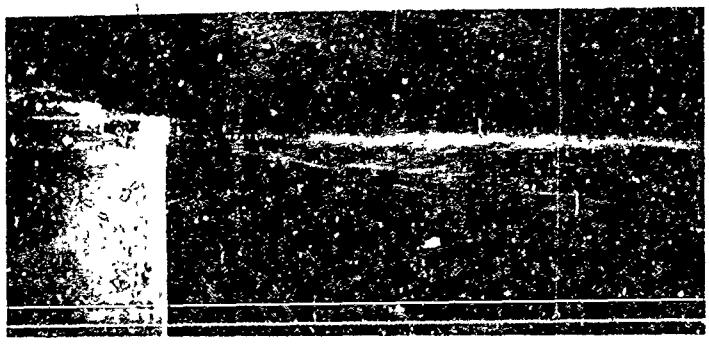

$m_i = 0.0027$ lb/sec

$m_i = 0.0037$ lb/sec

$m_i = 0.0046$ lb/sec

Figure 28. Change in the Trailed Vortex With Mass Injection; 3/16-L Nozzle; V=75 ft/sec; α=15°.

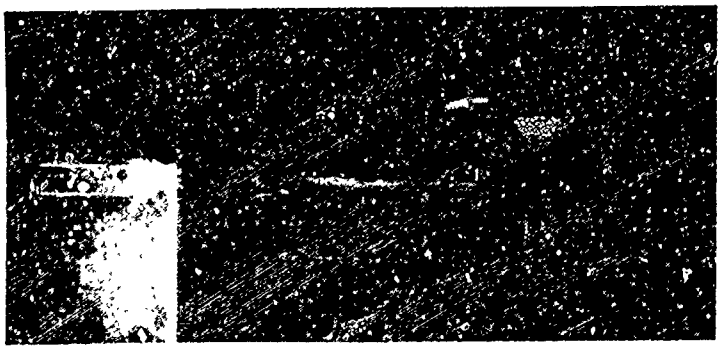

$m_i = 0$

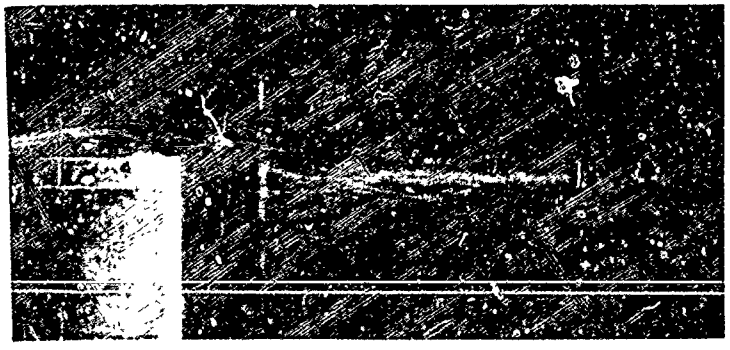

$m_i = 0.0019$ lb/sec

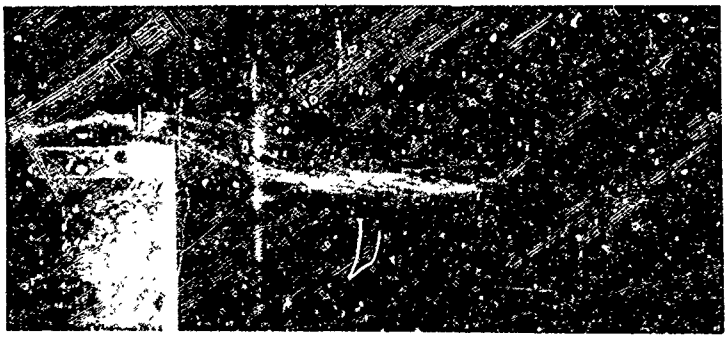

$m_i = 0.0025$ lb/sec

$m_i = 0.0031$ lb/sec

Figure 29. Change in the Trailed Vortex With Mass Injection; 1/8-S Nozzle; V=75 ft/sec; α=15°.

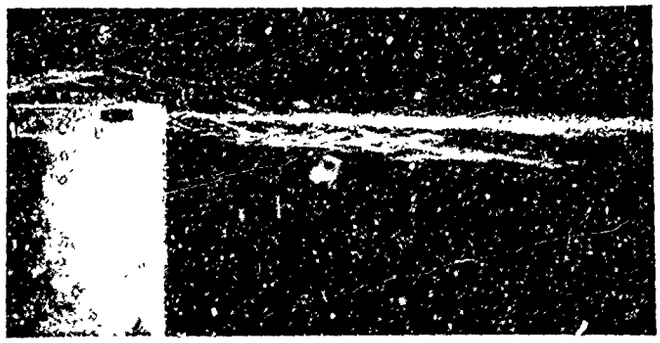

$m_i = 0$

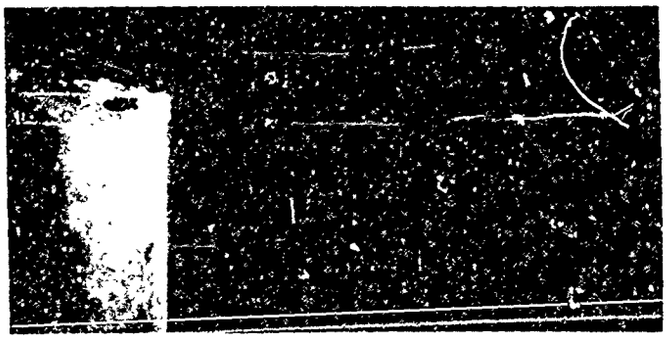

$m_i = 0.0019$ lb/sec

$m_i = 0.0025$ lb/sec

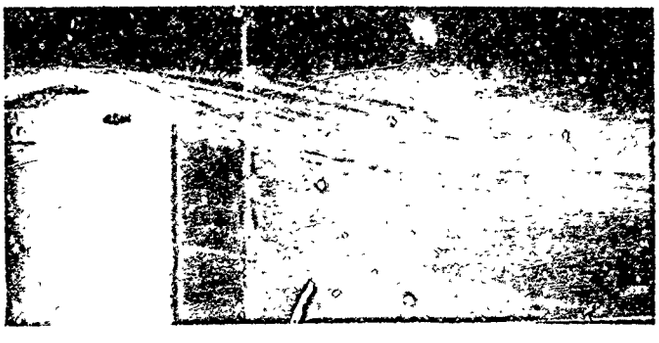

$m_i = 0.0031$ lb/sec

Figure 30. Change in the Trailed Vortex With Mass Injection; 1/8-L Nozzle; V=75 ft/sec; α=15°.

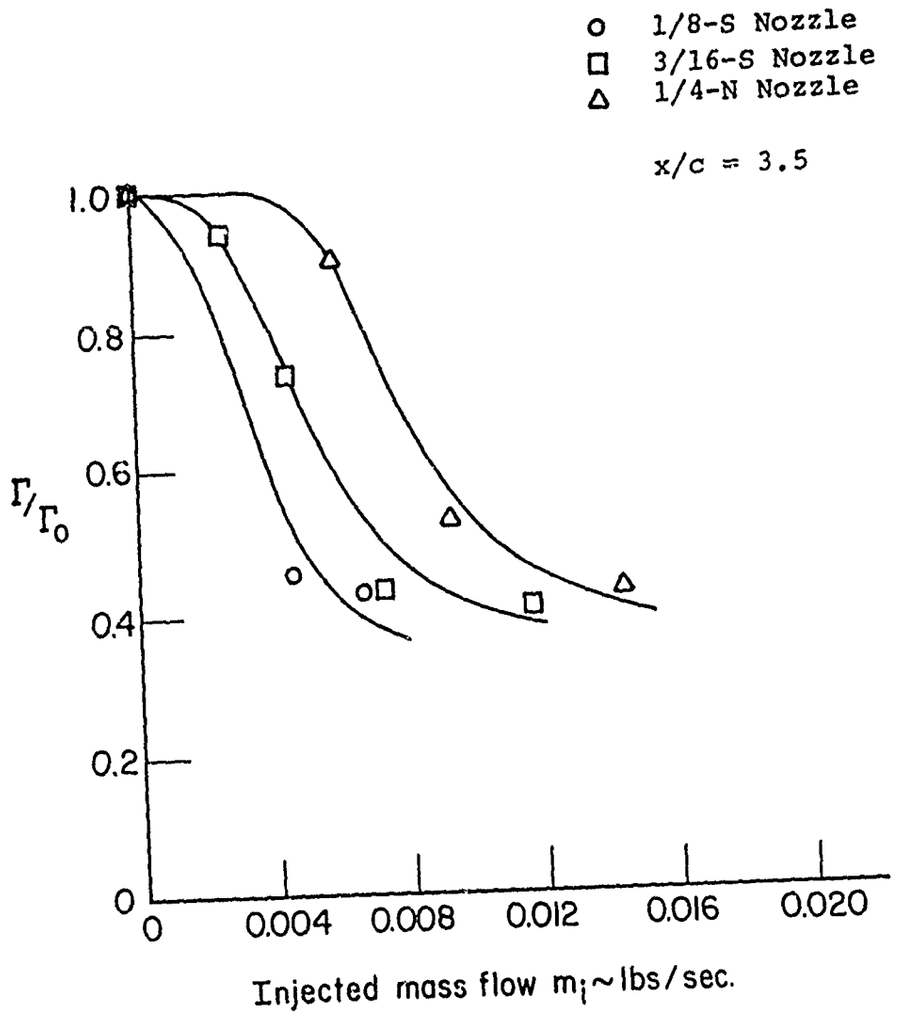

Figure 31. Γ/Γ_0 Versus Injected Mass Flow for Injection Tube Nozzles; V=75 ft/sec; α=15°.

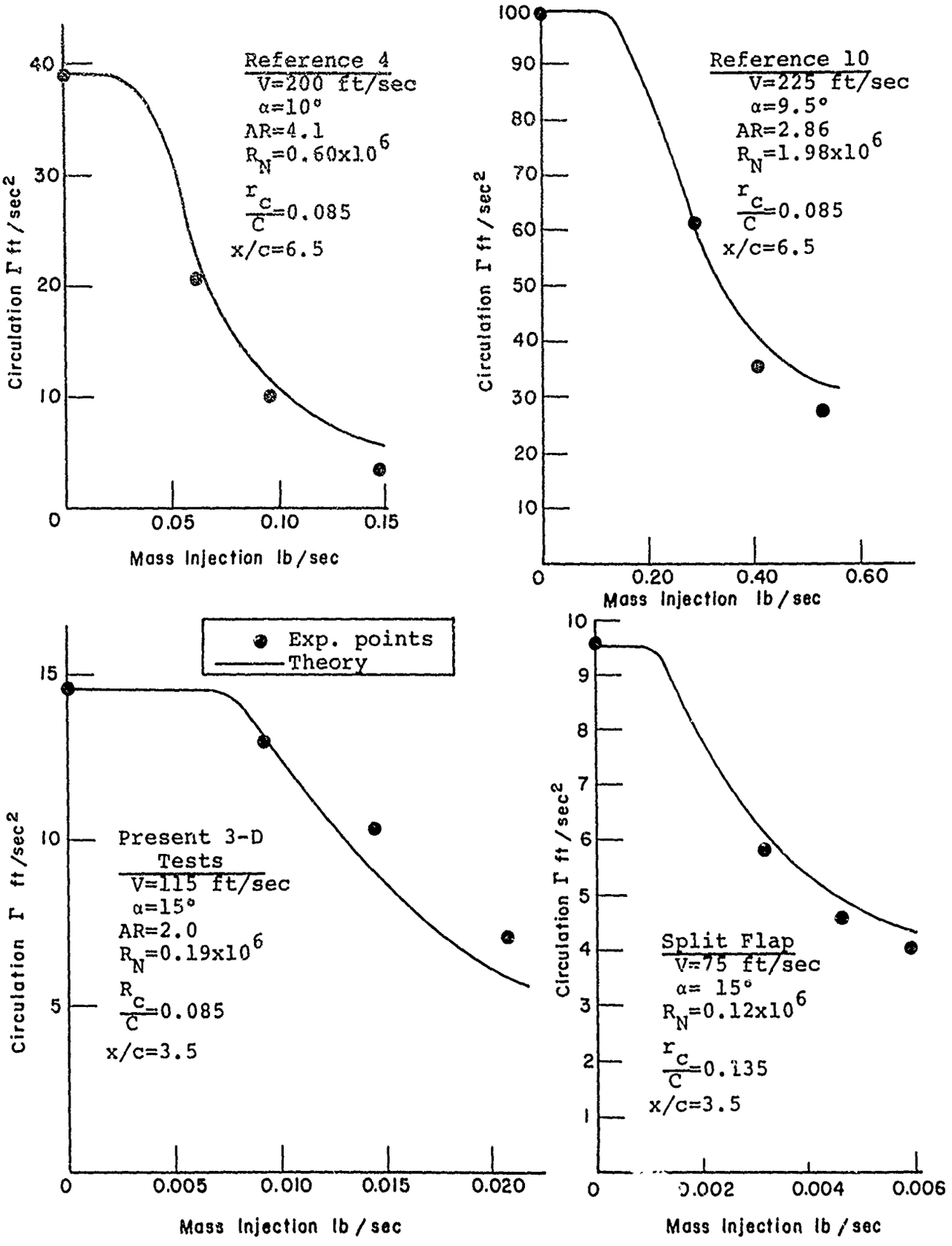

Figure 32. Comparison of Inductive Theory With Various Experimental Data.

APPENDIX

APPLICATION OF LINEAR MASS INJECTION TO CIRCULATION-CONTROL AIRFOILS

Circulation-control airfoils generally consist of cambered and noncambered elliptical-section airfoils with spanwise slits near the trailing edge. Air blown out of the slits provides lift augmentation for the airfoils. Since the source for air mass injection of the tip vortex is already available in the case of the circulation-control airfoils, it is desirable to determine not only the requisite blowing requirements to obtain a high lift-to-drag ratio by means of circulation control for these airfoils, but also the change in these requirements in order to eliminate the detrimental effect of the trailing tip vortex. The purpose of the investigation reported on in this appendix was to use existing results, and evaluate the characteristics of the flow field and the tip vortex generated by a circulation-control airfoil, and to relate these characteristics to conventional airfoils in regard to vortex injection.

The nondimensional pressure coefficient across the airfoil chord for circulation-control airfoils at section lift coefficients of 1.0, 2.0 and 3.0, which were obtained from the pressure distributions given in Reference 11 are shown in Figure 33. The distribution for C_L=0.5 was obtained by extrapolation of the data in this reference, and represents the pressure distribution with no lift augmentation. In this case, the airfoil is at zero angle of attack and the pressure differential is due to camber. The peaks in the pressure coefficients near the trailing edge at lift coefficients for 1.0, 2.0, and 3.0 are due to blowing which provides the lift augmentation.

Figure 34 shows the pressure distribution for a conventional NACA 0015 airfoil, which was obtained from Reference 14 at a lift coefficient of 0.5, and for the circulation-control airfoil of Reference 11 with no blowing (where C_L=0.5) and at the blowing

rate required to make C_L=2.0. For the NACA 0015 airfoil, a large pressure coefficient exists at the leading edge that rapidly drops off to C_p=0.6 at the 30% chord. Thereafter, it tapers off to zero at the trailing edge. In contrast, the pressure coefficient for the circulation-control airfoil with no blowing rises rapidly back to about the 20% chord. From x/c=0.20 to x/c=0.85, changes in C_p are more gradual and C_p is fairly constant with an average value of 0.6. By comparing the curves for C_L=0.5, it is obvious that a larger and more uniform pressure difference exists behind the quarter chord for the circulation-control airfoil. Since vortex wrap-up begins at about the quarter chord, a tighter vortex may thus develop from the circulation-control airfoil.

It has been observed in References 9 and 10 that the tip vortex for a conventional airfoil at a given angle of attack separates from the airfoil at about x/c=0.75. Since a circulation control airfoil will be at a lower angle of attack than a conventional airfoil for a given lift coefficient, there will be less tendency for the vortex to separate from the airfoil. The C_L=2.0 curve in Figure 34 shows low pressure near the trailing edge due to blowing through the jet slot. This lower pressure will also tend to delay the separation of the vortex from the airfoil surface. Thus, circulation-control airfoils will generally operate with their tip vortices remaining attached nearer to the trailing edge, and so the nozzle for vortex injection should be placed parallel to the chordline with its exit at the trailing edge.

Variations of lift coefficient with momentum coefficient for circulation-control airfoils as measured by Williams and Howe (Ref.11), Englar (Ref.12), and Yuan et al (Ref. 13), each for a different cross section, are shown in Figure 35. The momentum coefficient C_μ is defined by

$$C_\mu = \frac{\dot{m}V_j}{q_\infty c}$$

where m = mass efflux per unit length, slugs/sec ft,

V_j = jet velocity, ft/sec,

q_∞ = free stream dynamic pressure, lb/ft^2,

and c = chordlength, ft.

If the mass flow for vortex injection is obtained by tapping into the duct then the exit velocity and density will be determined by the existing duct pressure. Given the mass flow required for dissipation, the nozzle area is then determined by

$$A_{noz} = m_i/\rho_{noz}\, V_{noz}$$

where m_i is the injection mass flow rate.

For compressible flow, the jet Mach number will be

$$M = \sqrt{\frac{2}{\gamma-1}\left[\left(\frac{p_{td}}{p_\infty}\right)^{\frac{\gamma-1}{\gamma}} - 1\right]} = 2.2361\sqrt{\left(\frac{p_{td}}{p_\infty}\right)^{0.2857} - 1} \qquad \text{(A-1)}$$

where $\gamma = 1.40$ = specific heat ratio for air,

p_{td} = total duct pressure, lb/ft^2,

and p_∞ = free stream static pressure, lb/ft^2.

If p_{td}/p_∞ is less than 1.89 so that the flow is unchoked, the momentum coefficient will be

$$C_\mu = 2(h/c)\, M^2/M_\infty^2 \qquad \text{(A-2)}$$

where h = slot height. Equations (A-1) and A-2) were obtained from relations listed by Englar (Ref.12). The nozzle density is obtained from Bernoulli's equation

$$p_{noz} + \frac{1}{2}\rho_{noz}\, V_{noz}^2 = p_{duct}$$

and the pressure-density relation

$$p_{noz} = \rho_{noz}\, RT_{noz} \quad .$$

From these it is evident that

$$\frac{\rho_{noz}}{\rho_{duct}} = \left(\frac{p_{noz}}{p_{duct}}\right)^{1/\gamma} = \left(1 + \frac{\gamma}{2} M^2\right)^{-1/\gamma} .$$

The duct density is related to free stream density by

$$\frac{\rho_{duct}}{\rho_\infty} = \left(\frac{p_{duct}}{p_\infty}\right)^{1/\gamma}$$

so that we have

$$\frac{\rho_{noz}}{\rho_\infty} = \left(\frac{p_{duct}}{p_\infty}\right)^{1/\gamma} \left(1 + \frac{\gamma}{2} M^2\right)^{-1/\gamma} \qquad \text{(A-3)}$$

The tip vortex strength and the mass injection required to dissipate this vortex for several C_L's were measured in earlier tests conducted at NSRDC by RASA under a previous ONR contract (Ref. 4). The variation of tip vortex strength with C_L as obtained from these tests is shown in Figure 36. A first-order approximation of the mass injection required to dissipate the tip vortex to half of its noninjected value was found to be 3.4×10^{-3} lb/sec per unit of tip vortex strength.

In nondimensional terms, the required mass injection rate is

$$\frac{m}{\rho_\infty a_\infty c^2} = \frac{k}{\rho_\infty c} \frac{\Gamma}{V_\infty c} M_\infty$$

where $k = 3.4 \times 10^{-3}$ lb/ft^2. Since $m = \rho_{noz} A_{noz} V_{noz}$ it is obvious that

$$\frac{\rho_{noz} A_{noz} V_{noz}}{\rho_\infty a_\infty c^2} = \frac{k}{\rho_\infty c} \frac{\Gamma}{V_\infty c} M .$$

With $\rho_\infty = 0.0765$ lb/ft^3 this reduces to

$$\frac{A_{noz}}{c} = k' \frac{\Gamma}{V_\infty c} \frac{M_\infty}{M_{noz}} \frac{\rho_\infty}{\rho_{noz}} \qquad \text{(A-4)}$$

where $k' = 0.53$ inches.

Equation (A-4) gives the nozzle area which will supply the mass flow needed to dissipate the tip vortex. This nozzle area will vary when the lift coefficient is changed by adjusting the duct pressure. What is of interest is the variation of nozzle area with lift coefficient.

A summary of results obtained by applying these relations is presented in Figure 37, showing the minimum nozzle area required to dissipate the tip vortex versus C_L achieved by circulation-control. Note that the required tip nozzle area decreases at the higher C_L's although in these cases, the strength of the tip vortex would be greater. The reason for this is that a proportionately higher duct pressure and consequently higher mass flow is available for vortex injection at the higher circulation-control C_L values.

For determining the values shown in Figure 37 it has been assumed that for a given C_L the tip vortex strength is the same for a circulation control airfoil as that for a conventional airfoil. Although only limited pressure distribution data was available for this study, indications from this data are that for a given C_L, tip vortex strength may be somewhat greater in the case of a circulation-control airfoil. For this reason in practical applications it would seem advisable to use nozzle area values somewhat greater than those shown in Figure 37. Also it should be noted that only duct pressures (p_{td}) were considered which would result in unchoked flow through both the lift augmentation slot and the nozzle.

Figure 37 indicates that a nozzle area of $A_{noz} = 0.22$ inches times chordlength is adequate to eliminate the tip vortex for lift coefficients greater than 0.9. For example, a chordlength of 18" would require a nozzle area of 3.96 in.^{2}. This could be

achieved by using a 2.36-inch diameter tube. This diameter is 13% of the chordlength and would fit well in the 20% thick ellipse used by Williams and Howe.

The efficiency of dissipation is maximized when the velocity of injection is maximized. If a separate pressure supply is available for tip vortex injection so that the injection velocity can be kept near sonic velocity, mass flow requirements will be reduced significantly. In fact, if the injection velocity is only that produced by duct pressure, then the mass flow requirements for vortex dissipation may exceed the mass flow producing the lift augmentation.

For example, consider the case for a rotor blade with R=15' and c=1.5' operating at a tip Mach number of M_α=0.4 with C_μ=0.004. With h/c=0.00125, Equation (A-2) yields a jet Mach number of

$$M^2 = \frac{0.004 \times 0.4}{2 \times 0.00125} = 0.256$$

or

$$M = 0.505$$

Thus, the mass flow producing the lift augmentation is

$$m = C_\mu \, q_\infty \, Rc/V_j$$

$$= (0.004 \times 260 \text{ lb/ft}^2 \times 22.5 \text{ ft}^2 / 0.505 \times 1170 \text{ ft/sec}))$$

$$32.2 \text{ lb}_m \text{ ft/lb sec}^2$$

$$= 1.28 \text{ lb}_m/\text{sec}.$$

For M=0.505, Equation (A-1) gives the duct pressure as

$$p_{td}/p_\alpha = \left[1 + \frac{0.256}{5}\right]^{3.5} = 1.191 \ .$$

Thus, Equation (A-3) shows the nozzle density to be

$$\rho_{noz}/\rho_\infty = \left[\frac{1+0.7 \times 0.256}{1.191}\right]^{-1/1.4}$$

or

$$\rho_{noz} = 0.0765 \text{ lb}_m/\text{ft}^3 \times 1.0072 \approx 0.0771 \text{ lb}/\text{ft}^3 .$$

For $C_\mu = 0.004$, C_L=1.00 as shown in Figure 35. For C_L=1.00 and M_∞=0.4, Figure 37 gives the ideal nozzle area as

$$A_{noz} = 0.210" \times \text{chord} = 3.78 \text{ in.}^2 .$$

The nozzle injection velocity will be the jet velocity obtained earlier. Thus, finally,

$$m_{noz} = 0.0771 \times \frac{3.78}{144} \times 591$$

$$= 1.72 \text{ lb/sec} .$$

So, for this case, the ratio of injection mass flow to lift augmentation mass flow is 1.72/1.27 = 1.35.

The current tests with small diameter tubes(for which the injection velocity was large) showed that the mass flow required to dissipate the vortex to half of its noninjected value was 4.0×10^{-4} lb/sec per unit vortex strength. This value is 12 percent of that needed by other nozzles which operated at lower injection velocities. Thus, given a separate pressure supply so that injection velocity might be kept near sonic velocity, the required nozzle area for the preceding example would be 0.45 in.^{2}. The ratio of injection of mass flow to lift augmentation mass flow would then be 0.16 instead of 1.35.

In order to achieve an efficient design of a mass injection system for vortex dissipation of circulation-control rotors, an operating regime of the rotors should be established in terms of the circulation strength of the non-injected tip vortex versus angle of attack and the circulation-control mass flow requirements. Comparisons of the circulation strengths of these tip vortices with the injected vortices for various mass flows would establish the mass flow requirements for vortex dissipation. The mass injection system for dissipating

the tip vortex could be achieved by making provision for the installation of a tube into the tip of the model in such a manner that the vortex would be injected at its center and parallel to its centerline.

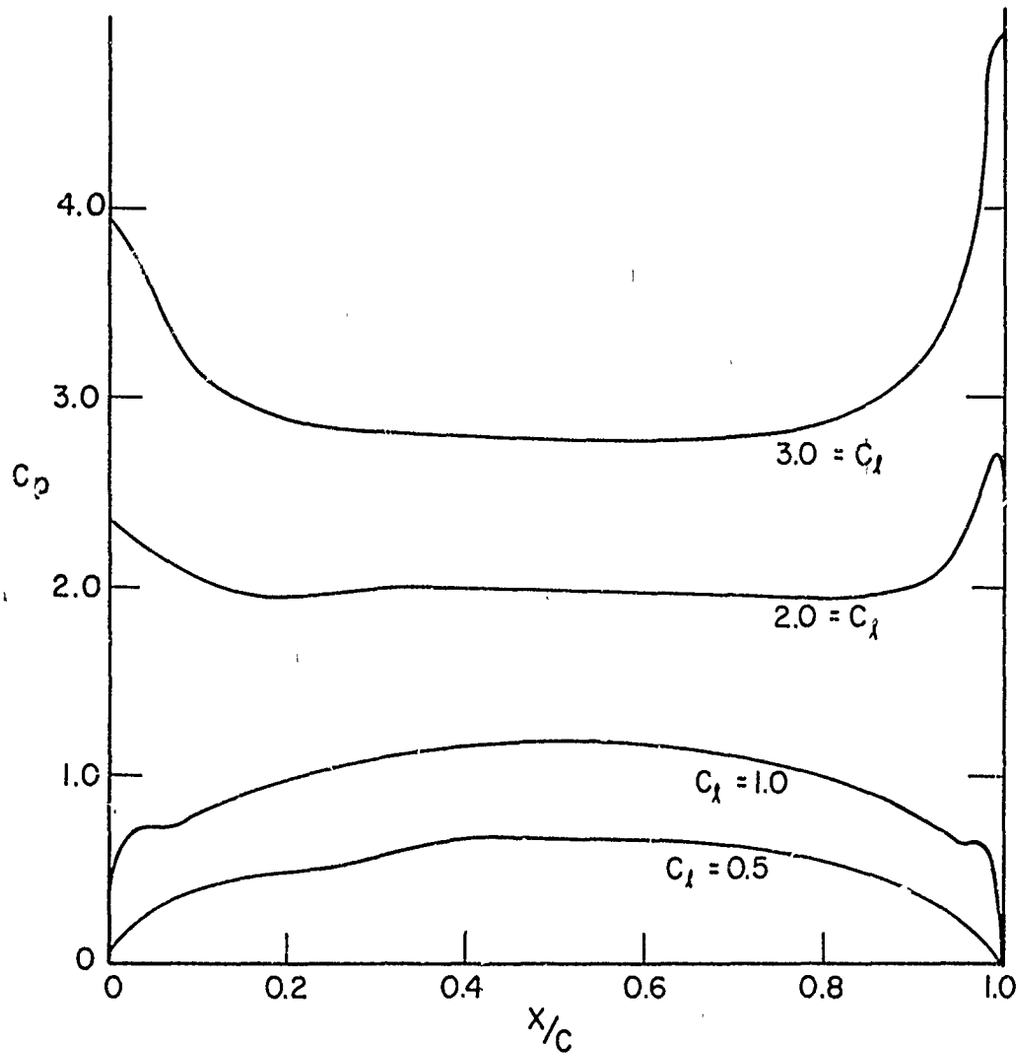

ure 33. Coefficient of Pressure Versus Chord of Circulatior-Controlled Airfoil for Various Blowing Rates.

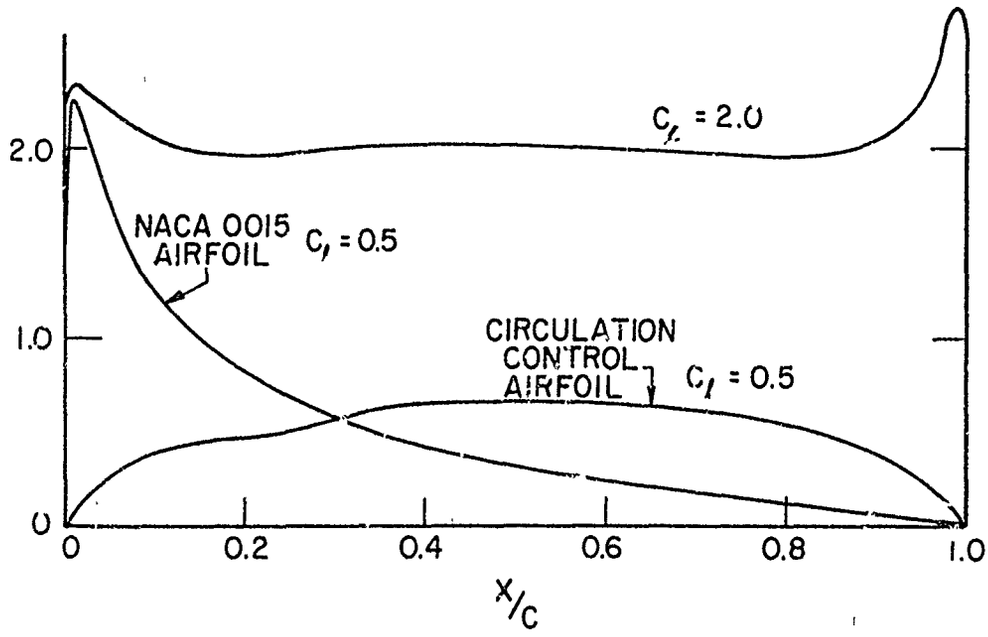

Figure 34. Comparison of Chordwise Pressure Distributions for Conventional and Circulation-Controlled Airfoils.

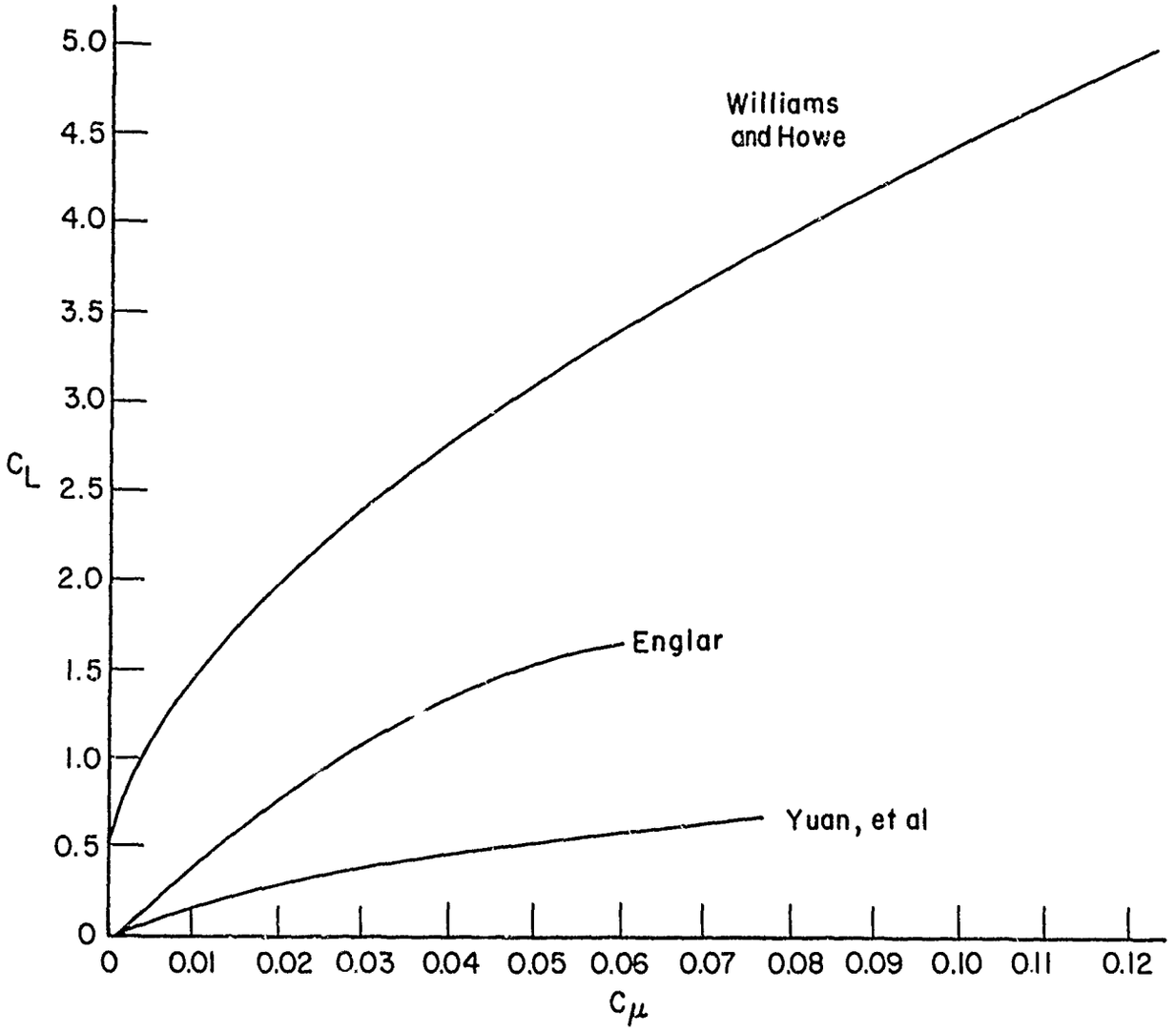

Figure 35. Coefficient of Lift Versus Momentum Coefficient.

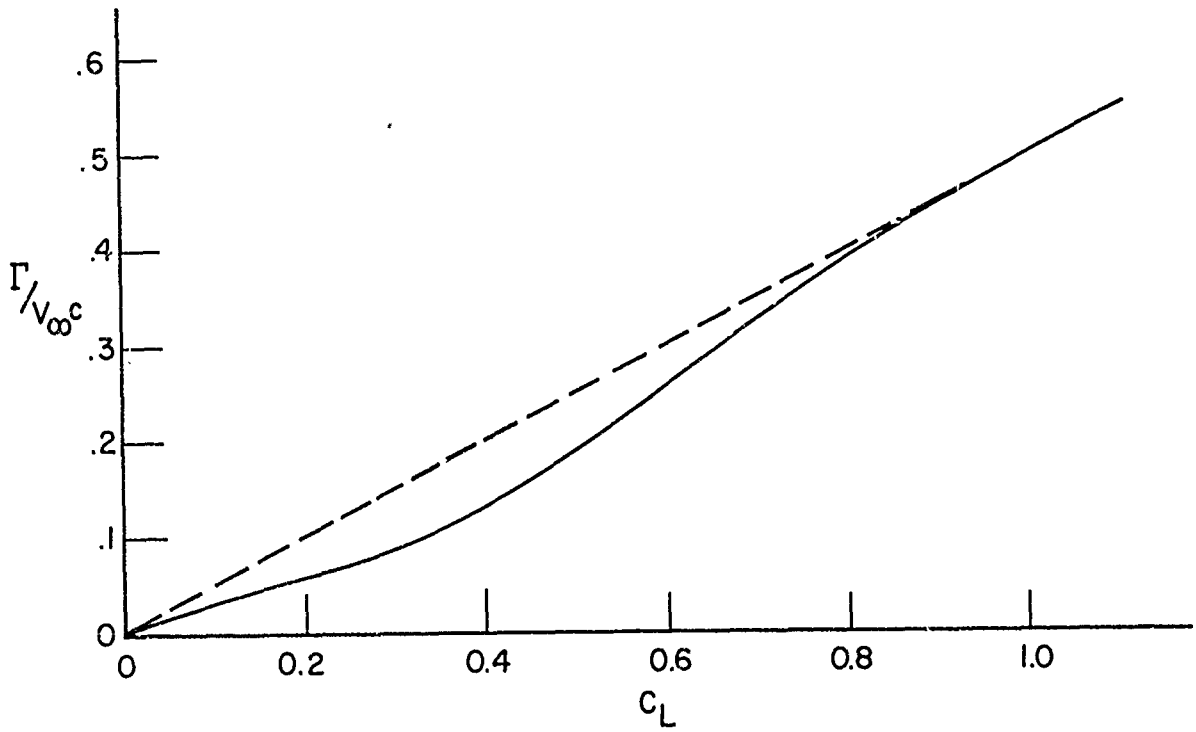

Figure 36. $\Gamma/V_\alpha c$ Versus Coefficient of Lift for Model of Reference 4.

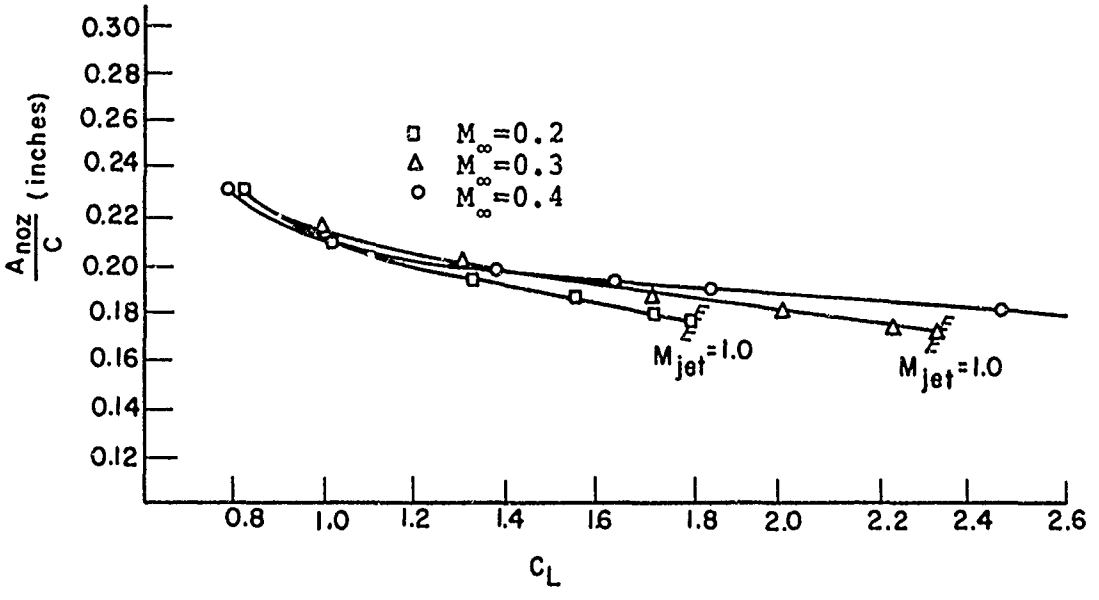

Figure 37. Minimum Nozzle Area for Tip Vortex Dissipation.